A STUDY OF ANOMALOUS EVENTS IN CMS-HF PMTs

by

Arda Halu

B.S., Physics, Boğaziçi University, 2006

Submitted to the Institute for Graduate Studies in
Science and Engineering in partial fulfillment of
the requirements for the degree of
Master of Science

Graduate Program in Physics
Boğaziçi University
2009

ACKNOWLEDGEMENTS

I want to express my deepest gratitude to Professor Erhan Gülmez for his guidance and assistance during the last one and a half year as my thesis supervisor. The insights he gave me and his endless patience proved invaluable throughout the whole process of preparing this thesis.

I would also like to thank fellow CMS Group member, teaching assistant colleague and friend Mehmet Deliömeroğlu for his priceless support, especially at the early phases of my thesis. With his advices, programming tips and moral support, I was able to overcome the initial challenges. I also thank my officemates and colleagues at the Department of Physics for the warm atmosphere they provided. Among my colleagues I would like to express my special thanks to Kazım Çamlıbel and Bora Işıldak for their true friendship in the last seven years and Fatih Erman for his help in my assistantship duties in the busiest semester of my academic life.

I gratefully acknowledge the Boğaziçi University Research Fund (No: 06B302) for their kind support in this work.

Finally and above all, I cannot thank my dear family enough for their perpetual support and encouragement, the peaceful environment they provided at home ever since my childhood and for being at times the sole reason for me to keep my spirits high.

ABSTRACT

A STUDY OF ANOMALOUS EVENTS IN CMS-HF PMTs

The Forward Hadronic (HF) calorimeter of the CMS detector will measure the hadronic jets as well as determine the missing transverse energy generally attributed to new physics phenomena. HF is a quartz fiber calorimeter in which the Čerenkov light generated by charged particles is collected by conventional photomultiplier tubes (PMT). In the HF test beam of 2004, events with unusually high energies with respect to the incoming beam energy were seen. These abnormal events were later confirmed in the 2007 test beam study.

In this thesis, anomalous events are studied in various aspects, with more emphasis on the comparison of their electromagnetic (EM) and hadronic (HAD) channel signals. EM/HAD and HAD/EM energy ratio histograms are plotted for several pion and muon test runs with different beam momenta. Incident tower ratio histograms in the typical energy range display a clear peak, justifying the existence of a correlation while histograms of abnormally high energy events for the sum of all other towers do not exhibit such a relation. This observation might help us infer that these anomalous events, which most probably result from particles striking PMT windows directly instead of passing through fibers to reach them, are of no experimental significance and may be tagged as “unreal” events to be discarded.

ÖZET

CMS-HF PMT'LERİNDEKİ ANORMAL OLAYLAR ÜZERİNE BİR ÇALIŞMA

CMS Dedektörü'nün İleri Hadronik Kalorimetresi (HF) hadronik jetlerin ölçümünde ve çoğunlukla yeni fiziksel olgularla bağdaştırılan dik yönde kayıp enerjinin belirlenmesinde rol oynayacaktır. HF, yüklü parçacıkların yarattığı Çerenkov ışığının konvansiyonel ışık çoğaltıcı tüpler (PMT) tarafından toplandığı kuvars fiber bazlı bir kalorimetredir. 2004 yılında HF üzerinde gerçekleştirilen test demeti çalısmasında, gelen demetin enerjisine kıyasla aşırı yüksek enerjili olaylar görülmüştür. Bu anormal olaylar 2007 yılındaki test demeti çalışmasında da gözlenmiştir.

Bu tezde anormal olaylar çeşitli yönleriyle incelenmektedir. Elektromanyetik (EM) ve hadronik (HAD) kanallardaki sinyallerin karşılaştırılması üzerinde özellikle durulmaktadır. Değişik momentumlarda çeşitli pion ve muon test demetleri için EM/HAD ve HAD/EM enerji oranı histogramları çizdirilmiştir. Demetin vurduğu bölme ve normal enerji aralığındaki olaylar için çizdirilen histogramlarda net bir tepe gözükmekte ve böylece bu olaylar için bir korelasyonun varlığı doğrulanmaktadır. Demetin vurduğu diğer tüm bölmelerde anormal yüksek enerjili olaylar için çizdirilen histogramlarda ise böyle bir korelasyon gözükmemektedir. Bu gözlem, anormal olayların büyük olasılıkla parçacıkların fiberlerden geçerek PMT'lere ulaşmak yerine doğrudan PMT'lere çarpmalarından kaynaklandığı, deneysel bir önem arz etmediği ve analiz dışı bırakılabileceği sonucuna varmamıza yardımcı olmaktadır.

TABLE OF CONTENTS

LIST OF FIGURES

LIST OF SYMBOLS/ABBREVIATIONS

atm	Atmosphere
c	Speed of light
E_T^{miss}	Missing transverse energy
fC	Femto Coulomb
f_{trap}	Trapped fraction of the Čerenkov light
GeV	Giga electron-volt
GJ	Gigajoule
H°	Higgs Boson
K	Kelvin
$m_{H^{\circ}}$	Mass of the Higgs Boson
MeV	Mega electron-volt
MHz	Megahertz
MV	Megavolt
n	Refractive index
ns	Nano second
T	Tesla
TeV	Tera electron-volt
γ	Photon
η	Pseudorapidity
λ	Wavelength
μ	Muon
μm	Micro meter
ν	Neutrino
θ_C	Čerenkov angle
$\widetilde{\chi}_i^0$	Neutralino
$\widetilde{\chi}_1^0$	Lightest Supersymmetric Particle
ADC	Analog-to-Digital Converter
AVP	Avalanche Photodiode

CMS	Compact Muon Soleoid
CSC	Cathode Strip Chamber
DAQ	Data Acquisition
DCC	Data Concentrator Card
DT	Drift Tube
ECAL	Electromagnetic Calorimeter
EM	Electromagnetic
HAD	Hadronic
HCAL	Hadronic Calorimeter
HB	Barrel Hadronic Calorimeter
HE	Endcap Hadronic Calorimeter
HF	Forward Hadronic Calorimeter
HO	Outer Barrel Hadronic Calorimeter
HPD	Hybrid Photodiodes
HTR	HCAL Trigger/Readout
L1	Level-1 Trigger
LHC	Large Hadron Collider
LSP	Lightest Supersymmetric Particle
NA	Numerical Aperture
QIE	Charge Integrator-Encoder
PMT	Photomultiplier Tube
PS	Proton Synchrotron
PSB	Proton Synchrotron Booster
RBX	Readout Box
RF	Radio Frequency
RPC	Resistive Plate Chamber
SPS	Super Proton Synchrotron
SUSY	Supersymmetry
TB	Test Beam
TS	Time Slice
WIMP	Weakly Interacting Massive Particle

WLS	Wavelength Shifter

1. INTRODUCTION

With an unprecedented center of mass energy of 14 TeV, the Large Hadron Collider (LHC) is expected to reveal new physics in many diverse fields. The Compact Muon Solenoid (CMS) is one of the two flagship detectors in LHC that has the capability of detecting many different types of particles with its dedicated subdetector components.

The focus of this thesis is on the Forward Hadronic Calorimeter (HF), which is a part of the Hadronic Calorimeter (HCAL) system in CMS. The main purpose of HF is to measure the hadronic jets at very high pseudorapidities and increase the overall efficiency in missing transverse energy measurements. The detection process in HF is through the generation of Čerenkov light and the transmission of this light to conventional photomultiplier tubes.

Test beam (TB) studies were conducted every year up to now on the calorimetry components of CMS. The data from these TB studies were analyzed by member institutions of the CMS collaboration for calibration, troubleshooting and optimization purposes. Events with abnormally high energies with respect to the test beam energy (an example being 600-700 GeV events in a 30 GeV pion beam) were noticed by A. Moeller *et al.* in the analysis of HF TB 2004 [1]. These anomalous signals were later confirmed in TB 2007 by A. Hunt *et al.* [2].

In this study, the aim was to devise a graphical approach to investigate the anomalous signals encountered in the test beam experiments. Data from the HF test beam study of 2004 were analyzed on the ROOT framework.

The thesis begins with a brief presentation of the Large Hadron Collider. The current status of the machine is also addressed. In the next chapter, the structure and physics goals of Compact Muon Solenoid is covered to introduce the reader to the detector. At the beginning of chapter four, some preliminaries on high energy physics calorimetry are given and hadronic calorimetry in CMS is described in detail in the remaining part of the chapter. In chapter five, the analysis regarding anomalous events is presented after a brief explanation of the analysis tools and experimental setup. The results are commented on in the final chapter.

2. THE LARGE HADRON COLLIDER

The Large Hadron Collider (LHC) [3] is the largest energy scale accelerator to date with a center of mass energy of 14 TeV, which surpasses its most recent predecessor, the Tevatron, by nearly an order of magnitude. It is primarily designed to produce proton-proton collisions although its programme also includes heavy ion collisions. Its main goal is to investigate electroweak symmetry breaking that is currently associated with the Higgs mechanism and to further test the consistency of the Standard Model at TeV energy scale. But as with all experiments in natural sciences, it may bring about other possible and exciting discoveries. Although Higgs boson is the most expected outcome, alternatives to Higgs mechanism that employ more symmetries, new forces and exotic particles, or even completely as yet unpostulated mechanisms may manifest themselves in the productive environment of TeV energies. Questions regarding dark matter, CP violation, antimatter and extra dimensions will hopefully also be answered to some extent.

2.1. Design and Construction

LHC is contained in the 27 km long and 3.8 m wide ring shaped tunnel originally built for CERN's previous large accelerator, the Large Electron-Positron Collider (LEP). The tunnel is located underneath the French-Swiss border and its depth varies from 50 to 175 meters depending on the geography.

The collider consists of eight arcs and eight insertion points. Arcs are where the bending dipole magnets reside and insertion points are where the particles are injected, dumped or cleaned; or where they collide (i.e. the detectors). The overall structure is divided into eight sectors and eight octants. A sector is the area spanning between two insertion points whereas an octant spans half of each arc with an insertion point in between. These two different partitioning conventions facilitate working with different parts of the machine.

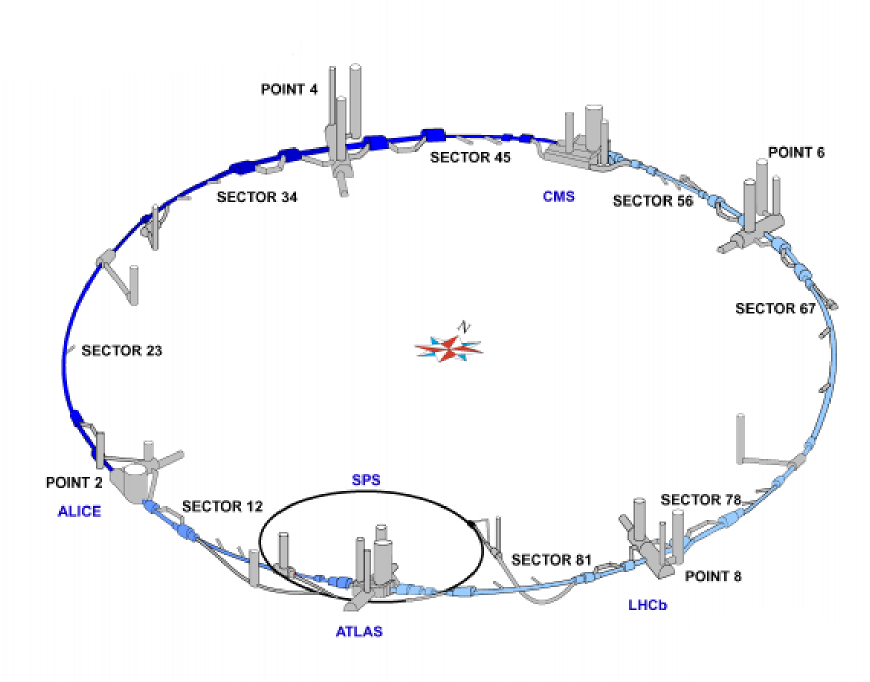

Figure 2.1. General view of the Large Hadron Collider.

There are a total number of six detectors located on the insertion points in LHC. Four of these, CMS, ATLAS, LHCb and ALICE, have dedicated experimental caverns while the other two small scale experiments, LHCf and TOTEM are built next to ATLAS and CMS, respectively. CMS and ATLAS are large, multi-purpose detectors that are able to cover a wide range of physics. LCHb specializes in b-quark studies. ALICE will analyze the heavy ion collisions. LHCf and TOTEM will investigate the very forward physics phenomena (Figure 2.1.).

2.1.1. Main Constituents

Beam: The beam is more like a train of particle bunches. There are 2808 bunches in one beam, each spaced 25 ns apart. In each bunch there are about 1.15×10^{11} particles. 25 ns spacing means a frequency of 40 MHz but the actual number of bunch crossings per second are less than 40 million (about 30 million) since larger gaps need to be left to allow for the operation of dump kicker magnets (Figure 2.2.). Since the collision cross section is very small, only about 20 collisions occur between the 200 billion particles of the opposing bunches. Multiplied with the 30 million crossings per second, we get about 600 million particle collisions every second in the LHC [4].

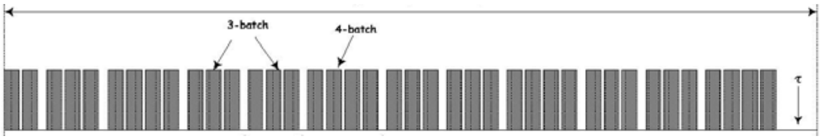

Figure 2.2. The bunch structure of the LHC beam. Notice the longer gap at the end.

Beam Pipe: There are two adjacent beam pipes, maintained at ultrahigh vacuum (10^{-13} atm), for the two opposing beams. The separate beams share the same pipe at the interaction points and are guided by magnets there for head-on collision. The pipes are encased in superconducting magnets, which are bathed in superfluid helium.

RF Cavities: The superconducting RF (radio frequency) cavities are responsible for accelerating the bunches and keeping them tightly together. There are eight cavities for each beam, each delivering 2MV at 400MHz. The cavities operate at 4.5°K. The "kick" provided by the resonating cavity increases the proton energy by 0.5 MeV in each turn.

Magnets: The LHC has a huge array of different types of magnets. The most important of these are the 1232 (154 in each arc) main superconducting dipoles that give the particles their circular trajectory, and 392 main superconducting quadrupoles that squeeze and focus the beam for better chances of collision. Together with the sextupoles, octupoles etc. and the auxiliary correcting magnets there are about 9600 magnets. The dipole field can reach the astonishing peak value of 8.33 T. The energy stored in all the magnets amount to 10 GJ.

Cryogenics: Cryogenics is utilized extensively throughout the LHC. Helium is the main cryogenic although liquid nitrogen is also used in cooling down the helium. The superconducting magnets are filled with helium that is cooled down to 4.5 K. Then the magnets are refrigerated further to 1.9 K for the helium to assume its superfluid state, acquiring very high thermal conductivity. 60 per cent of the 120 tonnes of helium is stored inside the magnets and the remaining part is shared between the distribution and refrigeration systems.

2.1.2. The Injection Scheme

Protons go through a succession of preaccelerators before being injected into the LHC. Protons obtained by ionizing hydrogen are accelerated to 50 MeV in Linac2 and then sent into the Proton Synchrotron Booster (PSB). Here the beam is accelerated to 1.4 GeV and fed into the Proton Synchrotron (PS) where its energy is further increased to 25 GeV. Next, the beam is injected into the Super Proton Synchrotron (SPS) and accelerated to 450 GeV before being finally transferred to the LHC. The beam circulates LHC for 20 minutes to reach the desired energy of 7 TeV [4].

2.2. The First Beam And Current Status

The first beam was injected into the LHC on September 10, 2008. First circulation of the beam was successful beyond anticipation in that it was completed in 55 minutes. The beam then went on to make two more full turns. After a minor repair on the cryogenics, the second beam in the opposite direction was sent and it too completed the loop in just over an hour. LHC continued single beam turns for a few hours until early afternoon and by late evening, LHC operations had managed 300 turns.

Given the seamless operation on the start-up day, the first modest energy (900 GeV) collisions were planned to be conducted in the last week of September. But on September 19, a quench in the superconducting electromagnets in sector 3-4 caused a helium leak into the tunnel, postponing the schedule. As the writing of this thesis is underway, the LHC is going through a down period that will last until mid-2009. The warming up of sector 3-4 has been completed and the transportation of the affected magnets to the surface has begun. In the expected scheme, all magnets will be up on the surface before Christmas shutdown and back in LHC at the end of March 2009. LHC is expected to be cooled back to superconducting temperatures and become operational again in July 2009.

3. THE COMPACT MUON SOLENOID

The Compact Muon Solenoid (CMS) [4, 5] is one of the two general purpose detectors in the Large Hadron Collider experiment which will study diverse physics phenomena at the TeV energy scale. Its surface complex is located in Cessy, France and its experimental cavern is directly underneath it at point 5 of the LHC (Figure 3.1.). CMS is expected to become operational by mid-2009, following the injection of the first beams in LHC.

3.1. CMS Goals

The many physics subjects that are within the scope of CMS can be summarized under the following categories [6]: the Higgs mechanism; supersymmetry (SUSY); dark matter; extra dimensions within the framework of string theory; antimatter and heavy-ion studies. There are numerous objectives for the CMS concerning these topics. These objectives will be briefly mentioned in the following subsections.

3.1.1. Discovery of the Higgs Boson

Higgs mechanism is an integral part of the Standard Model through which elementary particles are thought to acquire mass. Although originally conceived by P. Higgs to overcome a more general problem concerning symmetry breaking, it gained recognition after it was invoked by A. Salam and S. Weinberg in the revision of electroweak theory of S. Glashow to make up for the mathematical necessity that the gauge bosons should be massless, which was apparently a false prediction. It suggests that at a high enough temperature (a temperature that is comparable to that of the universe just after the Big Bang) all elementary particles except the so called Higgs boson are massless and when the temperature falls below a critical point a spontaneous symmetry breaking occurs, creating a Higgs field. The cosmos is believed to be dominated by the Higgs field ever since the Big Bang and elementary particles obtain masses proportional to the strength of their interactions with this field [6, 7].

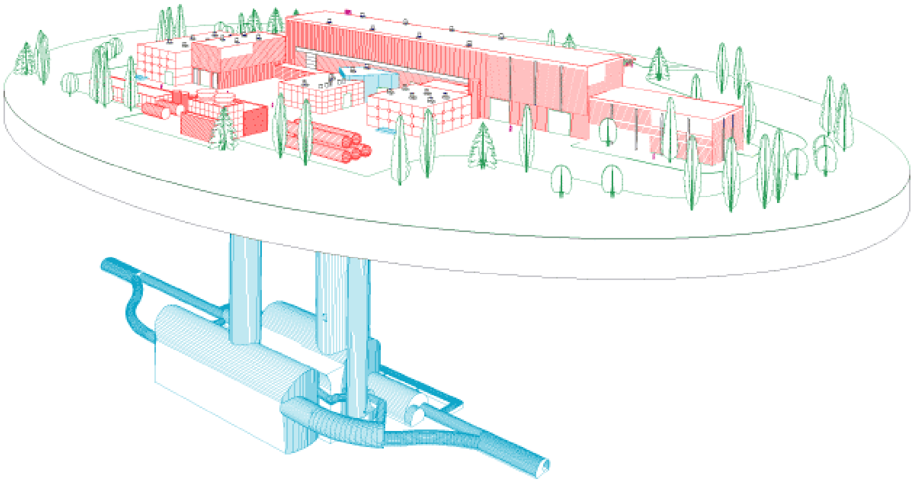

Figure 3.1. The surface complex and experimental cavern of CMS.

Since the Higgs boson hasn't been detected up until now, its mass is yet unknown. But the theory predicts the particle's decay modes and production rates for different mass ranges. There are more favored or more easily detectable decay modes in each range and the CMS has its several subsystems optimized for these modes. In fact, the various modes of Standard Model Higgs boson were used as benchmarks in testing the parts of CMS.

LEP had covered the mass range up to 114.4 GeV/c^2 for the Higgs boson, so the CMS will investigate the decay channels of higher masses. For 114 GeV/c^2 $< m_{H^\circ}$ $<$ 130 GeV/c^2 the H° $\rightarrow \gamma\gamma$ decay channel is the most promising channel. The high resolution electromagnetic calorimeter (ECAL) will play a crucial role in detecting the products of this mode. The most distinctive signature in the range 150 GeV/c^2 $< m_{H^\circ}$ $<$ 180 GeV/c^2 is H° $\rightarrow W^+W^- \rightarrow 2\mu 2\nu$. For 160 GeV/c^2 $< m_{H^\circ} <$ 600 GeV/c^2, decay into two Z's which in turn yield four leptons is the mode of choice. In these two channels the muon tracking system will do most of the job. If the mass of the Higgs boson is higher than 600 GeV/c^2, the favored channels will be the ones where Higgs decays into two W's or Z's which decay into leptons, jets and E_T^{miss} [4]. The hadronic calorimeter (HCAL) will detect these modes (Figure 3.2.).

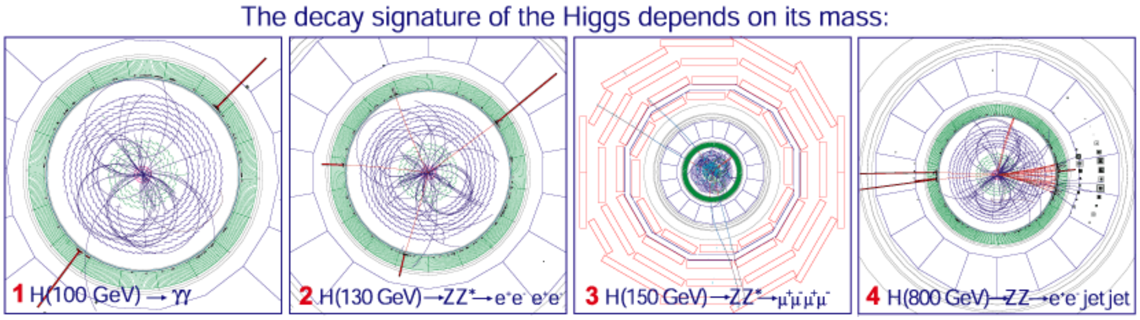

Figure 3.2. Some decay signatures of the Higgs Boson for various Higgs masses.

3.1.2. Search for Evidence of Supersymmetry

Devising a unification scheme that will bring together the electromagnetic, weak and strong forces and ultimately gravity is one of the highest reaches of physics, and not surprisingly the most difficult one. It is thought to be possible that these fundamental forces may be unified at extremely high energies. But even for the unification of electroweak and strong forces, i.e. not taking into account gravity, the order of magnitude of these energies way exceeds the energy scale of the LHC or any other previous experiment. Supersymmetry is an alternative line of thinking that utilizes symmetry to make unification of forces much more plausible, at experimentally accessible energies.

In supersymmetry, all Standard Model particles have supersymmetric partners (or “superpartners”) that differ by their spins. Fermions have superpartners that have integer spins and bosons have superpartners that have half-integer spins. So in a way SUSY predicts a symmetry between matter (fermionic) and force (bosonic) particles. It is believed to be a type of broken symmetry, which causes the SUSY particles (sparticles) to be much more massive and much less stable than their Standard Model counterparts. Naming convention is as follows: superpartners of fermions have an “s” in front, e.g. selectrons, squarks; superpartners of bosons take “ino” as a suffix, e.g. gluino, photino (Figure 3.3.). The theory is unable to predict the masses of superpartners but the various interaction signatures of superpartners can be identified within the theory[8, 9].

What CMS looks for as the evidence of supersymmetry is the Lightest Supersym-

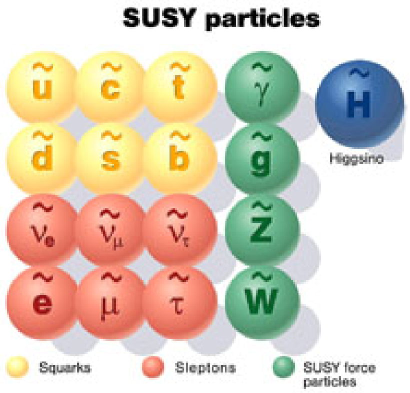

Figure 3.3. The Standard Model SUSY particles.

metric Particle (LSP). It is the lightest of four hypothetical particles called neutralinos (denoted by $\tilde{\chi}_i^0$ where i runs from 1 to 4) which are actually four distinct eigenstates formed by the mixing of four sparticles: a Zino, two Higgsinos and a photino. The decays of SUSY particles such as gluinos or squarks yield cascades that contain leptons and quarks and always the LSP (Figure 3.4.). Being weakly interacting and neutral, neutralinos are not directly observable in the CMS. The existence of LSP (denoted $\tilde{\chi}_1^0$) is deduced by the energy imbalance, as is the case with other neutral particles. CMS hadronic calorimeter (HCAL) measures this energy imbalance by adding up the transverse momenta of the resultant particles. Any missing transverse energy E_T^{miss} is either due to an undetectable particle or a detectable particle that somehow escaped the machine through non-detecting regions. The hermeticity of HCAL must be very good to ensure that E_T^{miss} really implies a neutral particle [6].

As in the case of Higgs bosons, there are several decay signatures from which the existence of SUSY particles can be deduced. The highest production cross section is for the pair production of squarks and gluinos. The final products of the three principal signatures are oppositely charged lepton pairs along with LSPs; quark and antiquark jets with two LSPs; and most notably, lepton pairs of the same charge which are generated by the decay of two gluinos each of which is equally likely to give positive or negative leptons. Several Higgs particles also appear within the framework of supersymmetry, and the decay modes of these Higgs particles will be investigated in CMS as well.

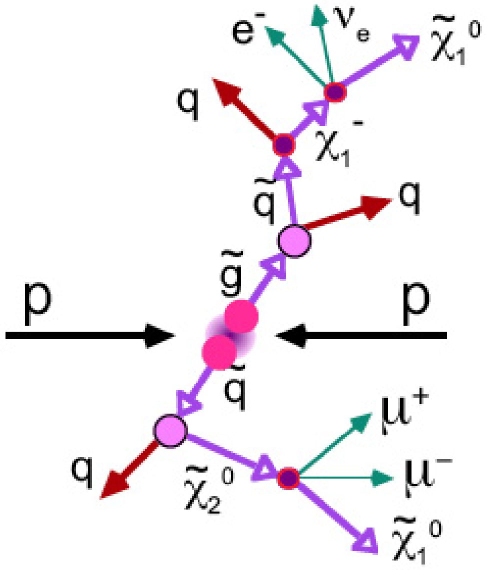

Figure 3.4. Production of LSPs (along with leptons) from the decay of SUSY particles.

3.1.3. Dark Matter Studies

Today we know through observational evidence that about 25 per cent of the energy density of universe is due to electromagnetically noninteracting hypothetical matter called dark matter. Compared with the 4 per cent of visible hadronic matter (the remaining 70 per cent is in the form of dark energy), this is too important a contribution to have gone unnoticed for so many decades. Historically the existence of dark matter was first implied in the work of Swiss astrophysicist Fritz Zwicky by the large discrepancy between the dynamic mass of a galaxy cluster, calculated using Newton's gravitation, and the luminous mass of the same cluster. According to the observed speeds of the galaxies which were much higher than anticipated, the mass had to be 400 times the observed (luminous) mass of the stars. In the early 1970s Zwicky's findings were affirmed when Vera Rubin showed in the galactic rotation curves for spiral galaxies that most of the stars rotated with nearly the same velocity regardless of their distance from the center (Figure 3.5.). The view that most galaxies are dominated with dark matter has gained wide acceptance and has continued up until today to be supported by more evidence from measurements of intergalactic diffuse gas and gravitational lensing, which is the process in which the gravity of a massive object such as a galaxy cluster acts as a lens distorting the light coming from distant galaxies

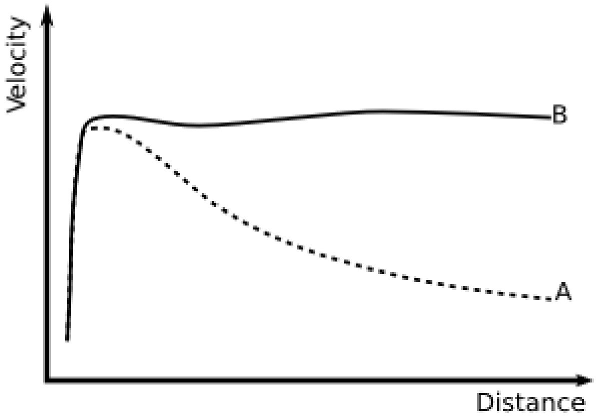

Figure 3.5. Galactic rotation curve of a spiral galaxy. A is the predicted curve whereas B is the observed one.

behind [10].

There are many candidates for dark matter which basically fall into one of the two categories: Baryonic and non-baryonic matter. Some of these candidates have been ruled out and the most favored candidates now are WIMPs (weakly interacting massive particles, of which neutralinos are members), axions and sterile neutrinos. CMS will be looking for neutralinos, specifically the LSP (mentioned in the preceding section), and if they exist and are detected they will help verify the dark matter theory as well [6].

3.1.4. String Theory and Extra Dimensions

String theory is one of the major theoretical physics fields whose aim is to deal with the notorious problem of reconciling general relativity and quantum mechanics, i.e. to describe the two in a single mathematical framework. In string theory, fundamental constituents are regarded as one dimensional extended objects –strings– that vibrate at resonant frequencies, instead of point particles. The strings are of Planck length (approximately 10^{-35} m) and each discrete vibration mode of the string corresponds to a different particle and the properties of the particle such as spin and charge and mass are governed by the string dynamics. Strings can be open as well as in closed loops. Although early versions of the string theory described only bosonic particles, modern versions now encompass superstring theories which invoke supersymmetry in order to include fermions in the picture.

The intriguing part of string theory is that mathematical consistency requires the existence of 10, 11 or 26 spacetime dimensions instead of the observed four. 26 dimensions appear in bosonic string theory, which is somewhat outdated; 10 dimensions are the prediction of superstring theories; and 11 dimensions appear in the M-Theory, which unites the five types of superstring theories and which is the most favored theory today as a candidate for the Theory of Everything. The six additional dimensions in superstring theory are all spatial. One way of visualising these extra dimensions is to think of every point in space as a six-dimensional manifold. The fact that they are extremely tiny (with each dimension of the order of Planck length) makes them undetectable by today's experimental means. Still, despite the abundance of alternative versions or equally possible solutions of the theory and the apparent difficulty of experimental verification, there are some ways in which CMS can contribute to the discovery of these dimensions [11].

One aspect of string theory predicts that heavier versions of particles should emerge recurringly at higher and higher energies as smaller dimensions are probed. These are called Kaluza-Klein recurrences. So the discovery of a known particle with greater mass could be evidence for extra dimensions. Another sign would be the disappearance of gravitons, manifesting in an imbalance in energy. This imbalance is very similar to the one that can be caused by SUSY particles, so the results should be analyzed thoroughly [6].

3.2. Design and Construction

The Compact Muon Solenoid takes its name from the solenoidal magnetic configuration chosen specifically for measuring the momentum of high energy muons. The detector consists of concentric layers of subdetectors that will measure the energy and momenta of different types of particles. These layers are (in order of increasing radius from the interaction point at the center): the silicon tracking system, the electro-

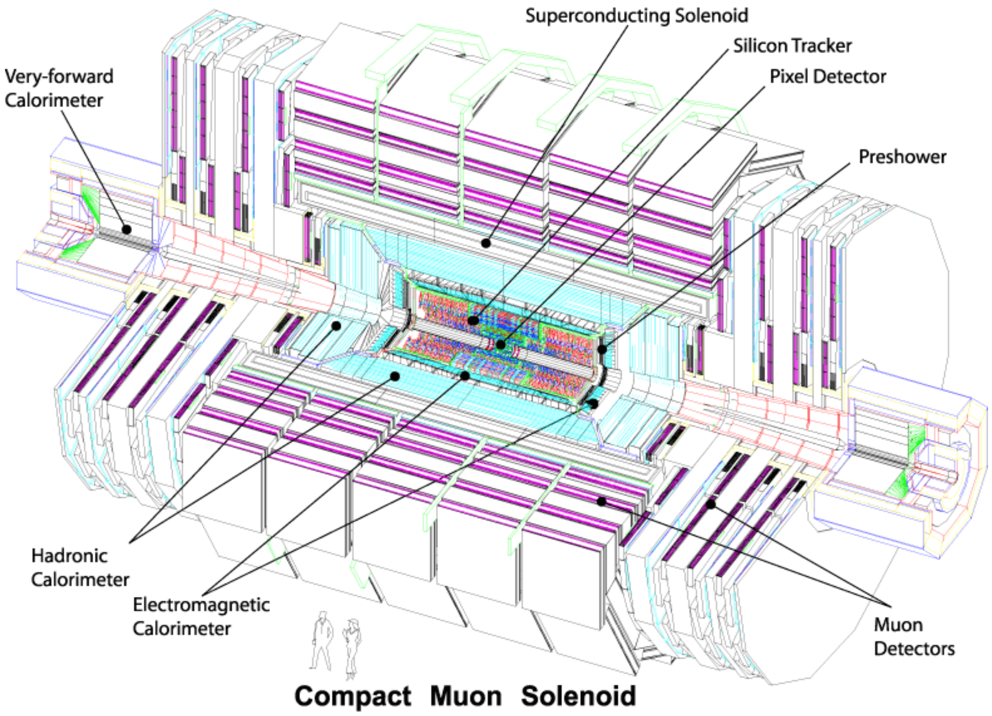

Figure 3.6. The subdetector components of CMS.

magnetic calorimeter (ECAL), the hadronic calorimeter (HCAL), the superconducting solenoidal magnet, the muon tracker - return yoke system. CMS measures 21 meters in length and 15 meters in diameter, weighing 12500 tonnes (Figure 3.6.).

It may be convenient at this point to mention the coordinate conventions adopted by CMS; thus the detector descriptions will hopefully be clearer. The nominal interaction point is accepted as the origin, with the x-axis pointing radially inward toward the center of the LHC and y-axis pointing vertically upwards. z-axis points along the beam line in the direction of the Jura Mountains from LHC Point 5. The azimuthal angle ϕ is measured from the x-axis in the $x-y$ plane. The polar angle θ is measured from the z-axis. Finally, a commonly used parameter is the pseudorapidity, defined as $\eta = -\ln\tan(\theta/2)$ [4].

3.2.1. The Silicon Tracker

The momentum of particles can be determined by measuring the curvature of their paths provided that magnitude of the magnetic field is known. The inner tracker of CMS can reconstruct the trajectories of the particles with very high precision. Since the tracker is the nearest layer to the interaction point, the prerequisite that it should withstand the severe radiation environment for several years led to a design based entirely on silicon technology. Given the design luminosity of LHC ($10^{34}\text{cm}^{-2}\text{s}^{-1}$), the tracker should also have a very high resolution and fast response in order to relate the particle paths with the correct bunch crossing.

The silicon tracker is made up of pixel and strip detectors. Three layers of cylindrical pixel detectors surround the interaction point, extending from 4.4 to 10.2 cm radially outwards. On the sides of the cylindrical tracker are two disk shaped endcap pixel detectors. The size of each pixel is $100 \times 150\ \mu m^2$ and there are a total number of 65 million pixels. After the pixel layers lie ten layers of strip detectors, between 20 and 116 cm. Four inner and six outer barrel strip detectors are completed by two inner and two outer endcap strip detectors. This part comprises 10 million microstrips overall. Particles striking the pixels or microstrips excite electrons from silicon atoms which are in turn collected and have their signals amplified. Thus a mapping of the particle trajectory in 2-D is possible knowing which pixels or microstrips have been hit. With the information from all of the tracker layers it is possible to reconstruct a 3-D picture of the particle trajectory.

3.2.2. The Electromagnetic Calorimeter

The electromagnetic calorimeter (ECAL) is the component of CMS that will measure the energy of electrons and photons emerging from the collisions. It is a hermetic homogeneous calorimeter consisting of a barrel part, two endcaps and additional preshower detectors. Specially designed radiation-hard and fast response lead tungstate (PbWO_4) crystals are used as scintillating material throughout the calorimeter. There are a total number of 75848 rectangular prism crystals varying in dimensions in different parts of the detector. Scintillation light from the crystals are captured by photodetectors attached to the back of the crystals. Avalanche Photodiodes (AVPs) are used as photodetectors in the barrel part whereas Vacuum Phototriodes (VPTs) are preferred in the endcap crystals due to higher pseudorapidity.

The preshower is a special section of the detector whose main purpose is to distinguish between high energy single photons (a signature of the Higgs boson) and closely spaced lower energy photon pairs (arising from the decay of a neutral pion). It is a sampling calorimeter consisting of two lead sheets that generate electromagnetic showers from incoming photons/electrons and silicon sensors placed after each lead sheet that measure the energy and position of the particles from the showers. The silicon sensors are divided into 2 mm wide strips enabling the preshower to have much finer granularity than the ECAL so that it can resolve the two lower energy photons that ECAL sees as one.

3.2.3. The Hadronic Calorimeter

The hadronic calorimeter (HCAL) is described in detail in the "Hadronic Calorimetry in CMS" section.

3.2.4. The Magnet

The specifications and field configuration of the CMS magnet was set by the muon detection requirements. A very strong magnet was needed in order to make accurate momentum measurements of even the highest energy muons. CMS utilizes a large superconducting solenoidal magnet that can attain a magnetic field of 4 T. It has dimensions of 5.9 m in diameter and 12.9 m in length. 2.7 GJ of energy is stored in the magnet at full current. A flux-return system integrated to the muon system complements the central solenoidal magnet. Three layers of iron return yokes are interleaved with the muon detectors to contain and return the magnetic flux. The return yokes also act as a filter, absorbing hadrons and letting through only muons and weakly interacting particles. The magnet weighs 12000 tonnes overall.

3.2.5. The Muon System

Precise and reliable detection of muons is one of the main design goals of CMS. The muon system is responsible for the identification and momentum measurement of muons as well as triggering. The muon system has, like the other subdetectors, a cylindrical barrel part and two endcaps. The structure consists of muon stations interleaved with iron flux-return yokes.

Three types of gaseous particle detectors are used in the CMS muon system. Drift tubes (DT) are preferred in the barrel part for muon position measurement. DTs cover the pseudorapidity range $|\eta| < 1.2$ where muon rate is low and the magnetic field is uniform. In the endcap regions where muon rate is high and the magnetic field is uneven, cathode strip chambers (CSC) are utilized, covering the region $|\eta| < 2.4$. A dedicated muon trigger system consisting of resistive plate chambers (RPC) are placed in both the barrel and endcap regions.

4. HADRONIC CALORIMETRY IN CMS

4.1. Calorimetry Overview

Calorimetry, as the name suggests, is the measurement of heat. The method originates from thermodynamics where it was used primarily to determine the specific heat of substances using thermally isolated containers called calorimeters.

In particle physics, however, calorimetry assumes a much broader meaning. In modern nuclear and particle physics experiments, calorimeters are complex devices that not only measure the energy of particles but also identify them and determine their many other properties. The terms calorimeter and calorimetry are used in the context of particle physics throughout the thesis.

The common feature of calorimeters is that the detection of particles is a destructive process, that is, the particles are completely absorbed by the calorimeter and are not available for further study. The absorption process is one in which the particles interact and lose energy while traversing the absorber material, generating secondary particles which in turn generate more particles and so on, resulting in a particle “shower” or “cascade” in the material. For this reason calorimeters are sometimes referred to as “shower counters”.

Calorimeters are of two types structurally: Homogeneous calorimeters and sampling calorimeters. In homogeneous calorimeters the part where the absorption of particles take place and the part where they are detected are the same. The material used has to have a high density to fulfill the first task. Sampling calorimeters are divided into two parts. The passive medium consists of a high density material (typically iron, copper, lead or uranium) that absorbs the particles whereas a separate active medium generates the signals from the particles [12].

4.1.1. Detection Mechanisms

Scintillation: Charged particles that pass through matter interact electromagnetically with the Coulomb fields of charged particles in the matter. The energy lost in this process can bring the atoms or molecules constituting the matter into an excited state. The excited states are unstable, however, and the excited atom or molecule quickly returns to the ground state, releasing the excitation energy in the form of photons. This process is called fluorescence or scintillation if the emitted photons are in the visible region. Scintillation timescales range from 10^{-12} to 10^{-6} seconds depending on the complexity of scintillator molecules; more complex molecules return to their ground states more quickly. Scintillators can be inorganic crystals as well as organic materials such as different plastic types.

Ionization: The energy lost by a charged particle when it is traversing a material may also ionize the atoms of the material, instead of just exciting them. Ionization detectors rely on the collection of the freed electrons from the ionization process to produce the detector signals. Ionization chambers may be based on liquid or gaseous media.

Čerenkov Radiation: Particles traversing a certain medium may have velocities (v) greater than that of light in that medium (c/n). When that is the case for a charged particle, it loses energy through an electromagnetic process called Čerenkov radiation. This radiation is emitted at a characteristic angle, $\theta_C = \arccos(1/n\beta)$, with the path of the particle where $\beta = v/c$. A cone of radiation is formed as a result, with a half-opening angle θ_C. Visible Čerenkov radiation is observed as blue light.

By studying the properties of the Čerenkov light a particle produces (i.e. the angle and intensity of radiation), the velocity of the particle can be calculated. If the momentum of the particle is also known, its mass can be determined, too. Particle identification is possible in this way.

Unlike the scintillation process, where signals are delayed due to factors such as the lifetime of the excited metastable state, Čerenkov radiation is continuous and instantaneous. This fact makes it an ideal choice for experiments demanding very high signal speeds.

4.1.2. Electromagnetic and Hadronic Showers

The dominating processes involved in the energy loss of particles determine the characteristics of a calorimeter. Electromagnetic and hadronic showers are produced as the result of combinations of these processes.

There are several processes that play a role in the energy loss (or absorption) of electromagnetically interacting particles (electrons, positrons and photons): Ionization of the absorbing medium, pair production, Compton scattering, the photoelectric effect and Bremsstrahlung. When a high energy electron traverses matter, it will radiate a large number of photons through Bremsstrahlung. The sufficiently energetic Bremsstrahlung photons will produce electron-positron pairs. The pair partners in turn will emit more Bremsstrahlung photons and so on. The result will be a shower containing thousands of electrons, positrons and photons [13].

In hadronic shower development, strong interactions between the shower particles and the nuclei of the absorbing matter are of great importance. The nature of the strong interactions make the hadronic showers much more complex than the electromagnetic showers. An inevitable complexity associated with strong interactions is the phenomenon of "invisible energy". Unlike electromagnetic interactions where all of the energy of the incident particle is deposited in the absorber, a fraction of the hadronic showers go undetected due to the production of non-interacting particles such as neutrinos.

If the hadron is charged, it will ionize the atoms of the matter it traverses, just like a muon or another electromagnetically interacting particle would do. But eventually the charged particle will meet an atomic nucleus with which it will interact via strong interactions. The hadron undergoes drastic changes (changes into several new hadrons, for instance) in strong interactions while the struck nucleus also changes (for example lose several neutrons and protons, ending up in a highly excited state, radiating several photons in turn). For neutral hadrons, ionization is not an option; they interact solely through strong interactions. The most frequently encountered neutral hadrons in hadronic showers are neutrons. The first generation of hadronic cascade products such as mesons, nucleons and photons may either ionize the atoms of the absorber or cause new nuclear reactions. The repetition of this process results in a hadronic shower.

4.2. The Hadronic Calorimeter

The hadronic calorimeter (HCAL) is the part of the CMS calorimeter system that is responsible for measuring hadronic jets and missing transverse energy, which is a signature of non-interacting, neutral particles. HCAL consists of four parts: Barrel (HB), endcap (HE), outer (HO) and forward (HF) calorimeter systems. HE and HB lie inside the solenoidal magnet, surrounding ECAL. HO is placed outside the solenoidal magnet and serves as a tail catcher to improve the containment of hadronic showers. The two HFs placed at each end of CMS cover the high pseudorapidity range and increase the overall hermeticity of HCAL.

HCAL is a sampling calorimeter with separate absorbing and detecting parts. Although differing in geometry, HB, HO and HE all consist of alternating layers of brass absorber as passive medium and plastic scintillator as active medium. In HB and HE, thickness of the scintillator layers is 3.7 mm whereas the thickness of brass plates vary from 50 to 78 mm. In HO the active layers have a thickness of 10 mm at the center rings. Particles incident on the brass absorber plates generate showers which are in turn picked up by scintillator sheets. Scintillator sheets are segmented into tiles of size $\Delta\eta \times \Delta\phi = 0.087 \times 0.087$, each coupled to a wavelength shifting (WLS) fiber. The waveshifters absorb the violet-blue scintillation light with λ between 410-425 nm to emit green light at $\lambda = 490$ nm. The waveshifted light is transported via clear fibers to readout boxes where the light signal is converted to electric signal by Hybrid Photodiodes (HPDs). HF is designed in a different way than the other three parts.

Details of HF is mentioned in the next section.

4.3. The Forward Hadronic Calorimeter

The two forward hadronic calorimeters (HFs) [4, 5, 14] are extensions of the HCAL system that are specifically designed to cover a pseudorapidity range $3 \leq |\eta| \leq 5$, thus improving the measurement of transverse missing energy and enabling the identification and reconstruction of very forward jets. E_T^{miss} measurement is of particular importance in CMS calorimetry since it may be indicative of SUSY particles or the Higgs Boson.

4.3.1. Structure

The primary concern in the design of HF was to choose suitable materials that could withstand the harsh radiative environment of the forward regions of CMS. The exceptionally high level of particle flux at these regions forbid the employment of waveshifter/scintillator materials that are used in ECAL and the other three sections of HCAL. Instead, steel absorber plates are used as passive medium and radiation-hard quartz fibers as active medium.

The quartz fibers consist of a fused-silica core with polymer hard-cladding. The fibers run through a succession of 5 mm thick steel absorber plates, parallel to the beam axis. Half of these fibers cover the full depth of the absorber (= 165 cm) while the other half starts at a depth of 22 cm from the front of the absorber. The use of long and short fibers help distinguish between electromagnetic particles and hadronic particles since electromagnetic particles deposit an important fraction of their energy in the first 22 cm of absorber. Long and short fibers are inserted alternatingly in the absorber and their signals are read out in separate channels.

HF is situated outside CMS, 11.2 meters away from the interaction point. It extends radially from 12.5 cm to 130.0 cm with respect to the center of the beam line. It is divided up into 18 wedges measuring 20° in ϕ (Figure 4.1.). The wedges in turn

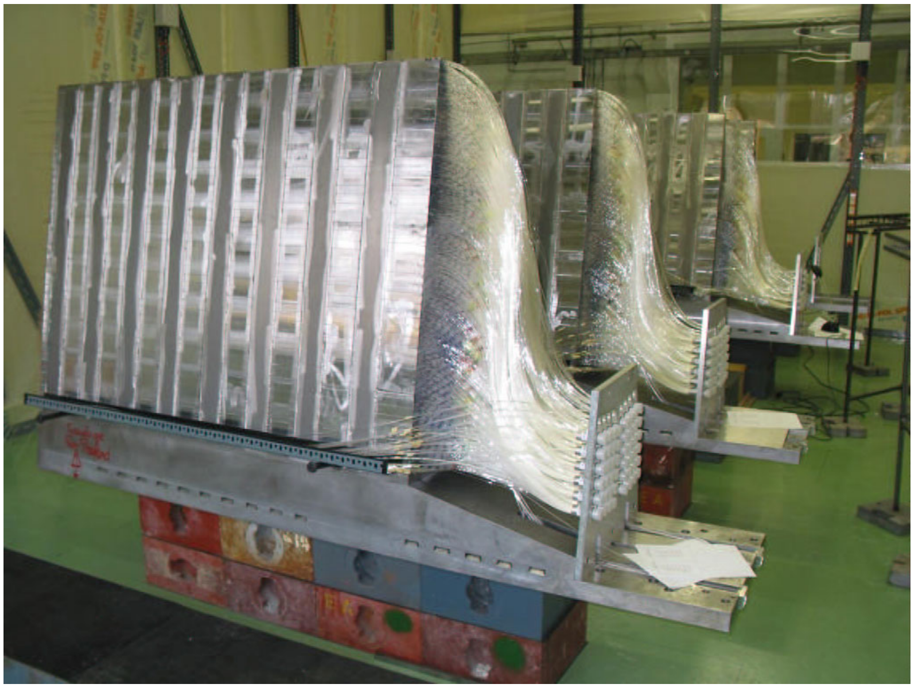

Figure 4.1. A picture of HF wedges where the quartz fibers emerging from the back of the wedge can be seen.

are segmented into “towers” of size $\Delta\eta \times \Delta\phi = 0.175 \times 0.175$ (Figure 4.2.). The fibers from each tower are bundled with the help of ferrules and connected to the air-core light guides inside a 42.5 cm thick shielding matrix.

When particles from the collisions in CMS are incident on the steel absorber, they generate particle showers. Charged particles from these showers with velocities above Čerenkov threshold generate Čerenkov light. A small fraction of the generated light (given by $f_{trap} = \mathrm{NA}/2n_{core}$ where NA (the numerical aperture) $= 0.33 \pm 0.02$) is collected and transmitted via fiber optics to the air-core light guides. Air-core light guides are hollow tubes coated on the inside with highly reflecting metal sheets that convey the light to the PMTs that are coupled to them. The light guides have a very high efficiency provided that the light is incident at $\approx 70^\circ$ from normal, but nevertheless nearly half of the light is lost in the process. PMTs are assembled in groups of 24 (one for each tower) in readout boxes (RBXs). There are two readout boxes for each wedge, corresponding to the electromagnetic and hadronic channels; so there are a total number of 48 signal channels in every wedge. The light guide/PMT/electronics assembly is housed separately behind steel, lead and polyethylene shielding.

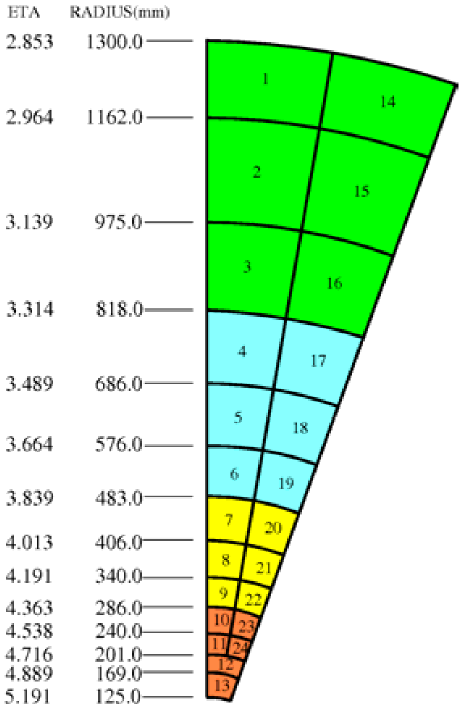

Figure 4.2. The HF tower structure.

4.3.2. Photodetectors and Readout Electronics

While readout electronics, triggering and data acquisition are sophisticated topics that are outside the scope of this work, it would be convenient to briefly point out the main guidelines for the data path and event structure, so that the codes run for the analyses can be better understood.

The light signals collected in HCAL detectors first go through an optical to electrical transducer to give analogue electrical signals. These signals are then digitized by specifically designed ADCs. The combined data from ADCs are sent to the triggering/readout board where packets of information including precision readout values and trigger primitives (the lowest step in the Level-1 triggering process – contains data about the energy deposits in calorimeter towers) are formed. The packets are finally sent to a data concentrator card (DCC) to be readied for transmission into the data acquisition (DAQ) system.

Level-1 (L1) Triggering in HCAL consists of three phases: Local, regional and global triggering. In local triggering, energy values from the calorimeter towers are added and the input data are linearized and filtered to form the trigger primitives. Regional triggering determines electron/photon candidates and transverse energy sums for each calorimeter region. Global triggering, being the highest level of L1 triggering, determines jets, total transverse energy and missing transverse energy.

In the case of HF, the optical to electrical converters are Hamamatsu R7525HA photomultiplier tubes. An application specific ADC called the QIE (Charge Integrator and Encoder) is used throughout the HCAL to convert analogue signals to digital. The QIE has four capacitors that are connected one at a time to the input (PMTs in this case) with a time interval of 25 ns. The charge from the capacitors are summed (integrated) and converted to seven-bit digital signal (encoded). The 32-bit data created with the contribution of three QIE channels along with some additional monitoring signals is sent to HCAL Trigger/Readout (HTR) boards. HTRs calculate the trigger primitive packets mentioned above and send them to Regional and Global Triggers. After the L1 triggering is complete, HTRs send the trigger primitives to data acquisition [4, 5].

4.3.3. Time Characteristics

The time characteristics of signals gain much more importance as the event rates get higher (for the LHC, event rates are of the order of a GHz). There are two aspects to the time characteristics of a signal: timing (synchronization) and duration. Timing is the accuracy with which a signal can be associated with a certain event or bunch crossing whereas the duration is the width of a signal in time. The duration of the signal depends on the particular shower production types and detection mechanisms involved. More than one of these showering types may contribute in different amounts to the overall time structure of a signal.

Signals are generated in HF through the emission of Čerenkov light, which is an extremely rapid process. Therefore the HF signals have a very short duration; typically 10 ns. Owing to the the extremely short duration of the signals, consecutive events that have a very short time in between can be successfully resolved by the quartz fibers used in HF. Another thing to note is that in HF, the difference between the arrival times of light at the upstream and downstream ends of the detector (165 cm apart) was measured to be 2.3 ns [12].

5. DATA ANALYSIS

In the analysis, a graphical approach was taken to investigate the abnormally high energy events. A series of histograms and scatter diagrams were plotted in ROOT by feeding in 2004 HF test beam data. A macro written for common usage in the analysis of TB 2004 (plotALLHF.C) was taken as basis and modified in several ways to generate the plots.

5.1. ROOT

ROOT is an object-oriented data analysis framework developed by CERN to better meet the needs of experiments like LHC where data will be produced at a rate higher than any other previous experiment. Unlike previous analysis platforms that were written in FORTRAN, ROOT was developed using the object-oriented approach. Although the emphasis is on data analysis, the ROOT framework encompasses many features and tools for data acquisition, event generation and reconstruction and detector simulation as well. ROOT uses a C++ interpreter and has packages for tasks such as histogramming, curve fitting, 3-D visualization and many more [15].

5.2. Test Beam 2004 and Experimental Setup

The HF test beam experiment of 2004 was conducted at the H2 beam line of the Super Proton Synchrotron (SPS) at CERN. A single HF wedge was placed on a specially designed table that could be moved horizontally and vertically with a very high precision. The table could also tilt the wedge vertically from the beam line between 0° to 6° to simulate the actual particle trajectories. One of the three types of beams (muon, pion or electron) at 30, 50, 100, 150 or 300 GeV was directed on a single tower of the wedge in each run. The tested wedges were 2-1, 2-2, 2-3, 2-4, 2-6, 2-13 and 2-14 [14].

5.3. Analysis

The analysis presented in this thesis is carried out with the presumption that the cause of the abnormally high signal yielding events seen in the test beams is most probably particles directly hitting the PMT windows instead of the intended process of being transmitted through the quartz fibers, losing energy via Čerenkov radiation. Since PMTs are devices that have exponential gain characteristics, resultant signals with very high values can be read out due to directly incident particles.

This anomaly in the detection process could manifest itself in a number of ways. One of these is related to the timing of the signals since there should be a discrepancy between the arrival times of particles passing through quartz fibers and particles directly striking the PMTs. So the first approach was to divide each event into 20 time slices and form 20 separate histograms for each time slice to see in which time interval the test beam was mainly on, and more importantly, if the abnormally high energy events appear in any other time slices. These histograms were plotted for the single tower the beam was incident on and the relevant channel (EM or HAD depending on the beam). Semi-log histogram type is preferred to clearly see the few anomalous events. (Figure 5.1.)

The separate time slice histograms were plotted for many pion and muon runs. As a result, no high energy events are seen in time slices other than the 6th and 7th, which were the time slices the beam was incident on. In time slices (TS) 6 and 7 though, few such events stand out clearly.

Next, since anomalous events were not seen in any time slice other than the 6th and 7th, these two time slices were investigated more thoroughly. To graphically view how the two are related, scatter diagrams were plotted with TS6 on the horizontal axis and TS7 on the vertical axis. The scatter diagrams in this part of the analysis were plotted separately for the tower the beam was incident on and the sum of all other 23 towers, for the related channel. Events with nearly the same energies are "binned" into groups and their energies in the respective time slice are marked. A scatter diagram

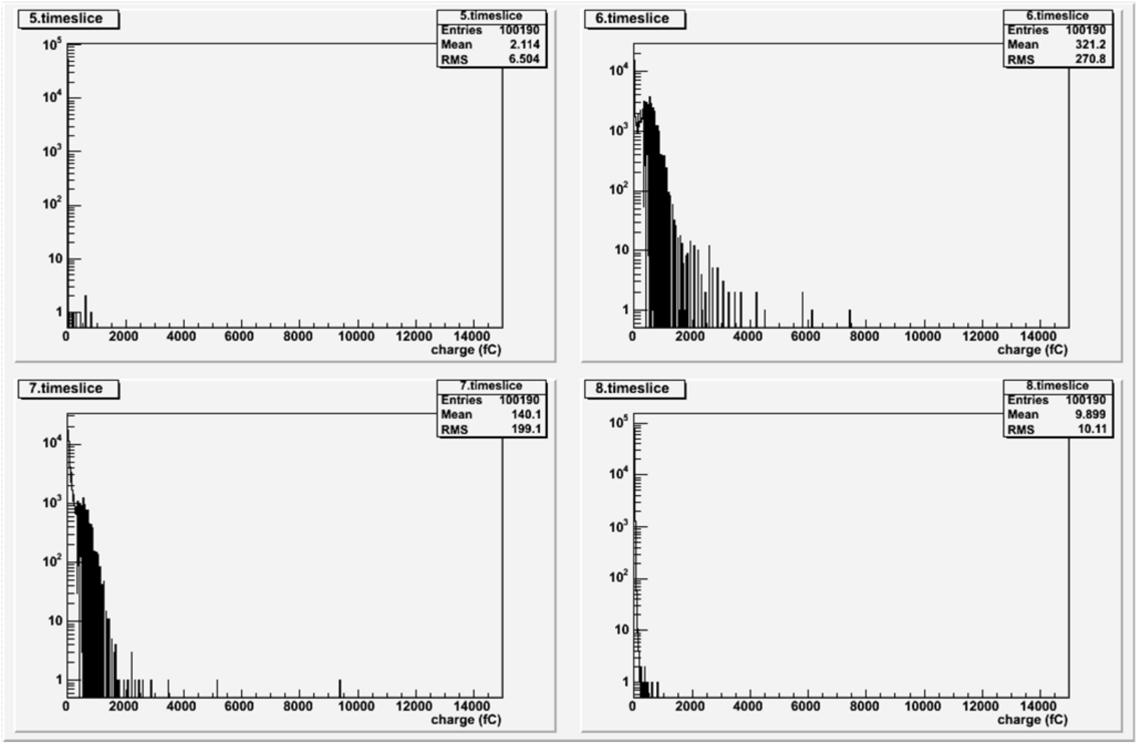

Figure 5.1. 100 GeV pion run, incident tower (tower 2), time slices 5 through 8.

type was chosen in ROOT in which different number densities are represented with different color tones.

For the incident tower diagrams, the hump-like formation near the horizontal axis is common for all the runs analyzed and can be regarded as characteristic. Meanwhile, a homogeneous distribution is displayed in the diagrams for the sum of all other towers, possibly due to the scarcity of statistics. And the few events with negative energies appear most likely due to pedestal related issues. (Figures 5.2. and 5.3.)

The previous sets of scatter diagrams indicated that an event can have energy values in both TS6 and TS7. In this part of the analysis, two histograms were plotted for each run for the relevant channel by excluding the energy values of these time slices from one another, i.e. by selecting events with zero energy in TS6 among events seen in TS7 and vice versa. This was done basically to learn more about events coinciding with the axes in the previous scatter plots. The rarity of such events are evident in the histograms and this observation tells that there must be a slight deviation from the axes as energy gets higher. (Figures 5.4. and 5.5.)

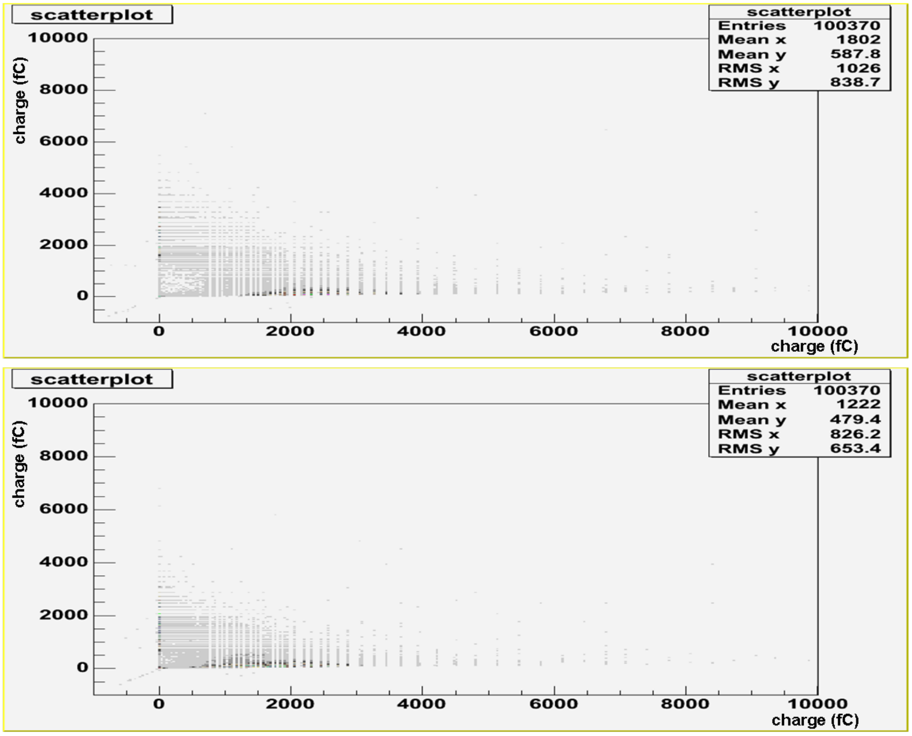

Figure 5.2. TS6 vs TS7 scatter diagram for a 300 GeV pion beam. Plotted for the incident tower (tower 2). EM (above) and HAD (below) channels.

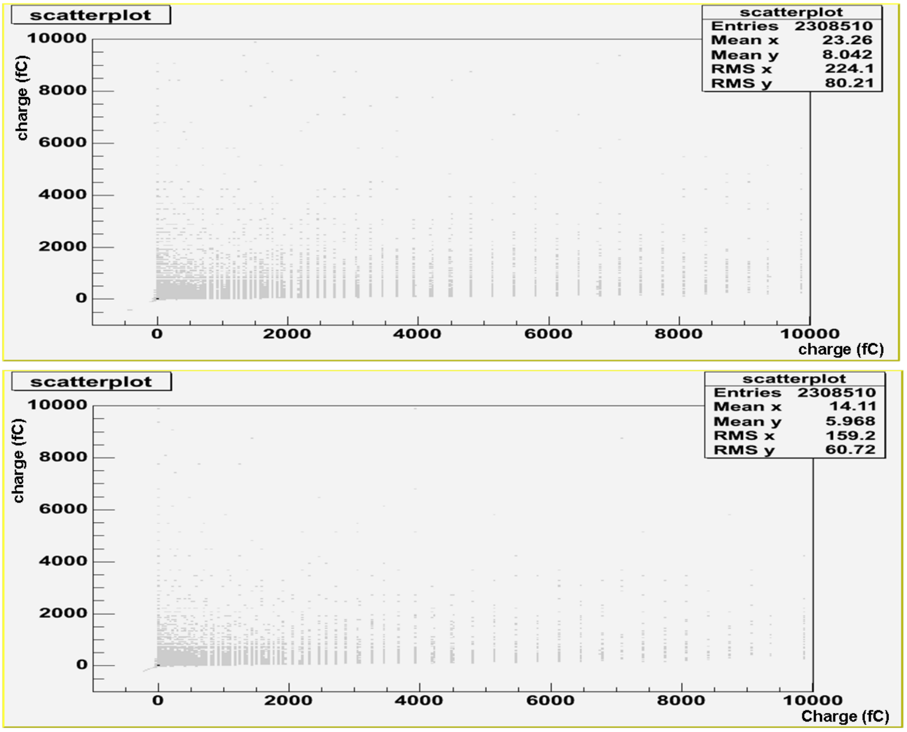

Figure 5.3. TS6 vs TS7 scatter diagram for a 300 GeV pion beam. Plotted for the sum of all other towers. EM (above) and HAD (below) channels.

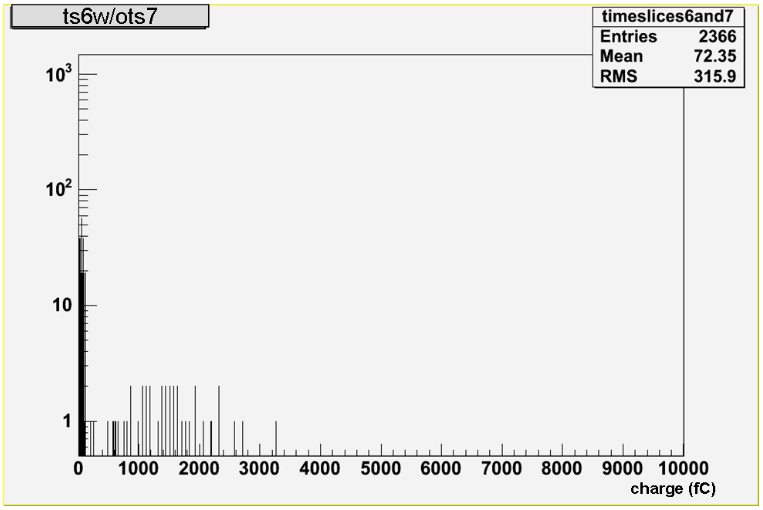

Figure 5.4. Histogram of TS6 events - TS7 excluded. 300 GeV pion beam. Plotted for the incident tower (tower 2).

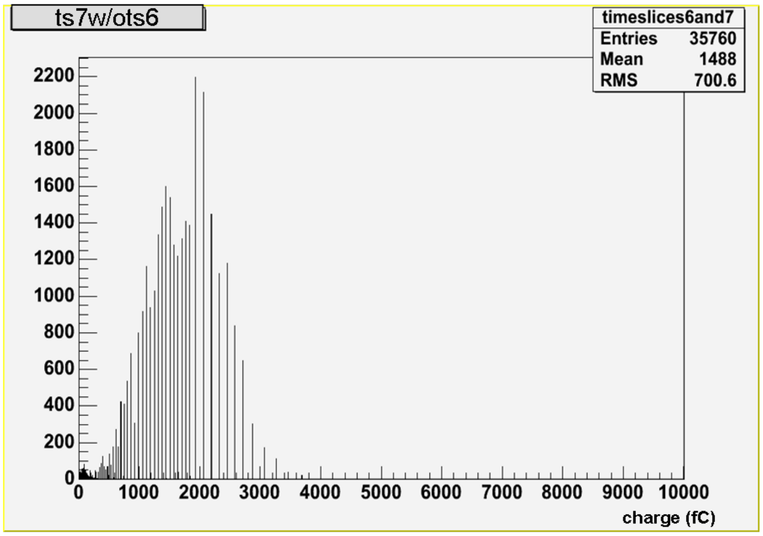

Figure 5.5. Histogram of TS7 events - TS6 excluded. 300 GeV pion beam. Plotted for the incident tower (tower 2).

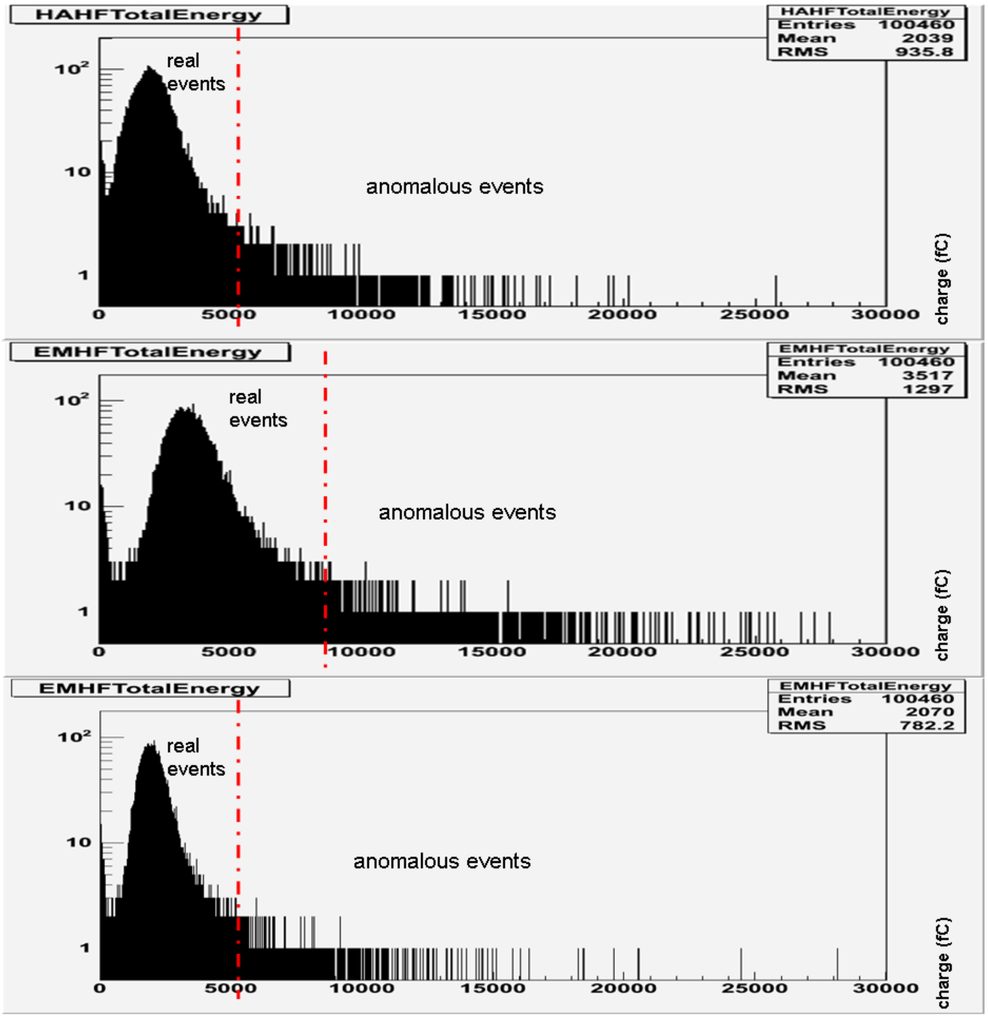

Figure 5.6. 300 GeV pion beam (run no: 15031), all towers. HAD channel, EM channel and normalized EM channel, respectively.

In the rest of the analysis, the focus of attention was shifted from time intervals to towers and channels. To see how EM and HAD channels compare in terms of the abnormal energy events, two histograms (one for each channel) were plotted for the sum of all 24 towers and the events were not divided up into time slices. Then, an additional EM histogram was plotted in which raw charge values were normalized with respect to the HAD channel (Figure 5.6.).

Next, scatter diagrams with EM channel on the horizontal axis and HAD channel on the vertical axis were plotted to look for signs of correlation between the two channels. Again, two separate diagrams were plotted for the incident tower and the sum of all other towers. (Figures 5.7. and 5.8.)

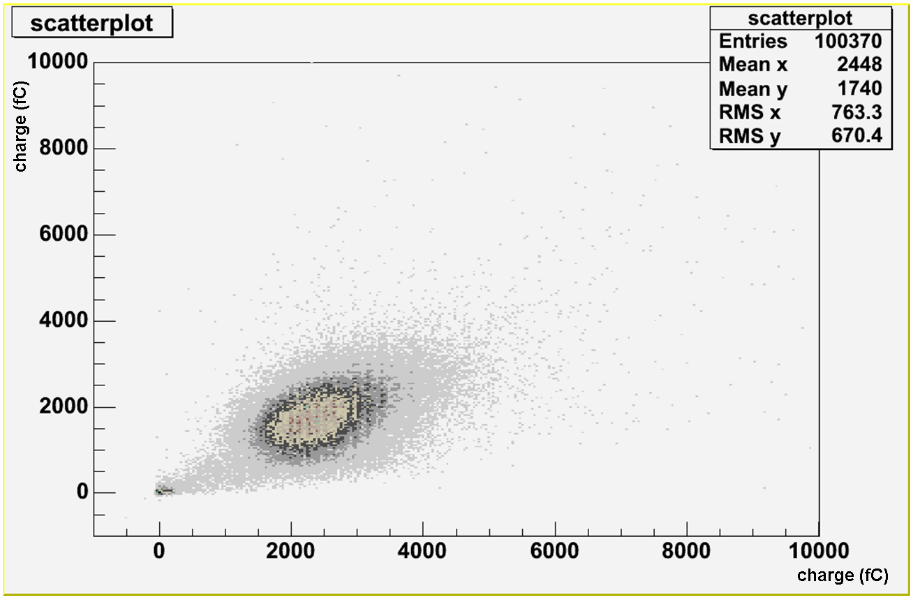

Figure 5.7. EM vs HAD scatter diagram for a 300 GeV pion beam (run no: 15030). Plotted for the incident tower (tower 2).

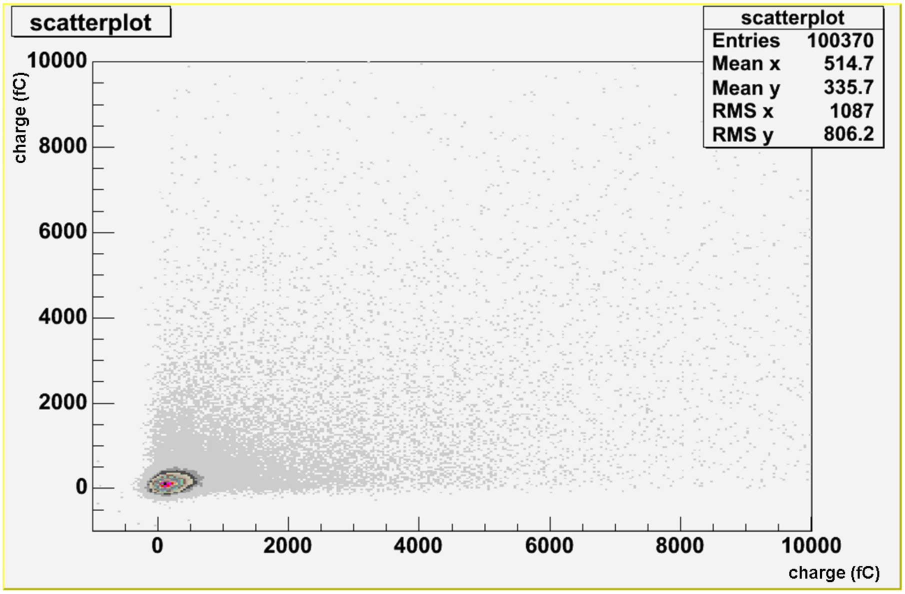

Figure 5.8. EM vs HAD scatter diagram for a 300 GeV pion beam (run no: 15030). Plotted for the sum of all other towers.

In the incident tower plots there is a clear correlation between the signals in EM and HAD channels of events in the normal energy region, hence the neat elliptical distribution. For the all-other-towers plots, the region near the origin is dense with events while in other parts a homogeneous distribution emerges again. Events constituting the axes (events with energies solely in EM or HA channels) can be seen clearly in the diagrams for some of the test runs, especially those of relatively low energy pion beams.

In the final part of the analysis, two sets of EM/HAD and HAD/EM signal ratio histograms were plotted: one for the tower the beam was incident on, in the expected energy range; and one for the sum of all other towers in the anomalous energy zone, that is, for $Q > 6000$ fC in either of the channels. The "expected" energy range is determined by referring to the EM vs HAD scatter diagram of the same test run. (Figures 5.9. and 5.10.)

As a result, the incident tower ratio histogram displays a clear peak, which proves the existence of a correlation between the two channels of normal energy events. The mean ratios are very nearly the reciprocals of each other. On the other hand, such a peak does not emerge in the all-other-towers histograms formed for the anomalous events. In addition to that, high ratios are quite common in these histograms. It is known that the EM and HAD channels of a real event yield comparable signals. The lack of such a correlation suggests that these events were not collected through the normal detection means of HF [16].

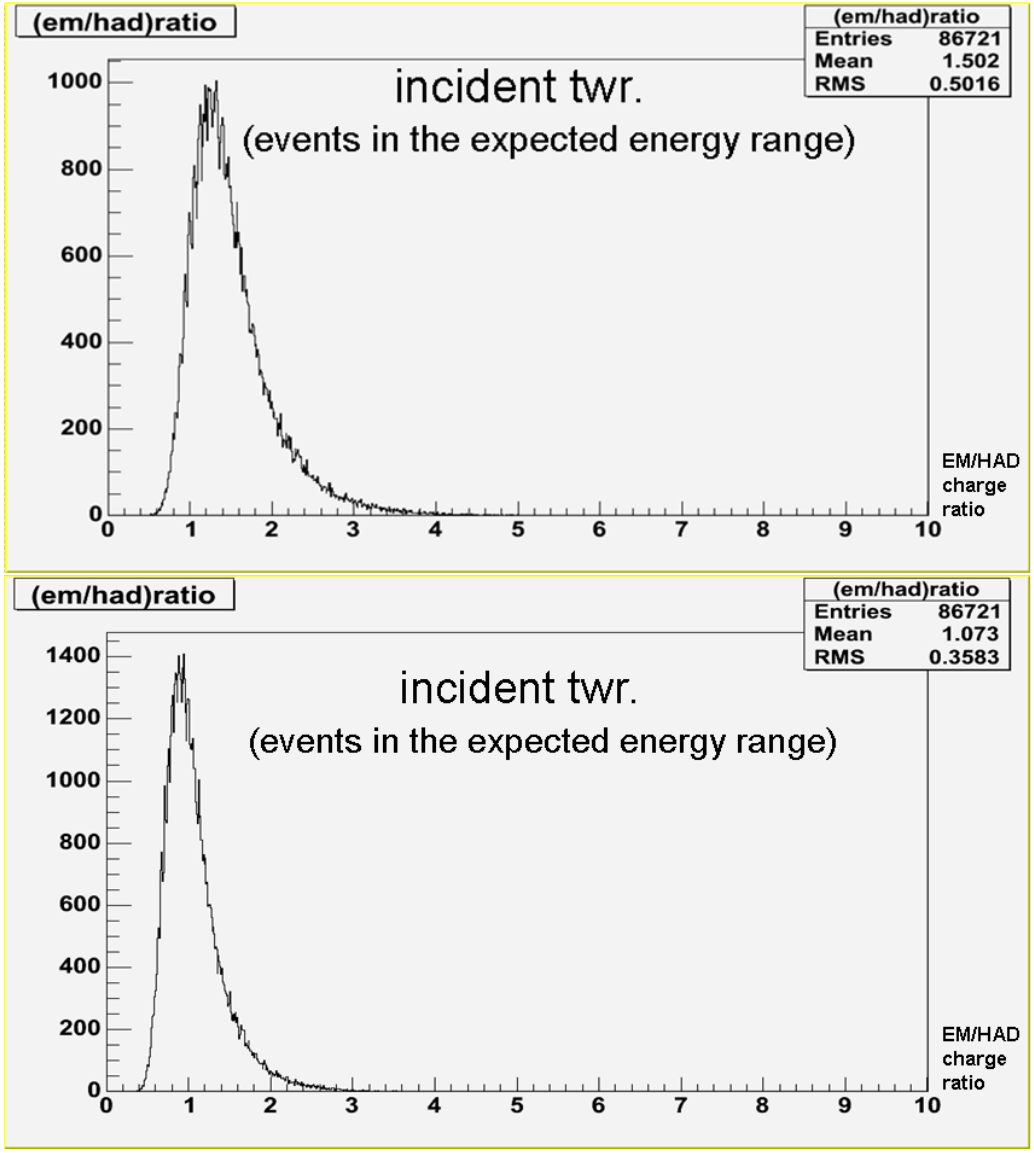

Figure 5.9. (Top) EM/HAD ratio histogram calculated with raw charge values. (Bottom) The same ratio histogram calculated with normalized EM charge values. 300 GeV pion run (run no: 15030). Plotted for the incident tower (tower 2).

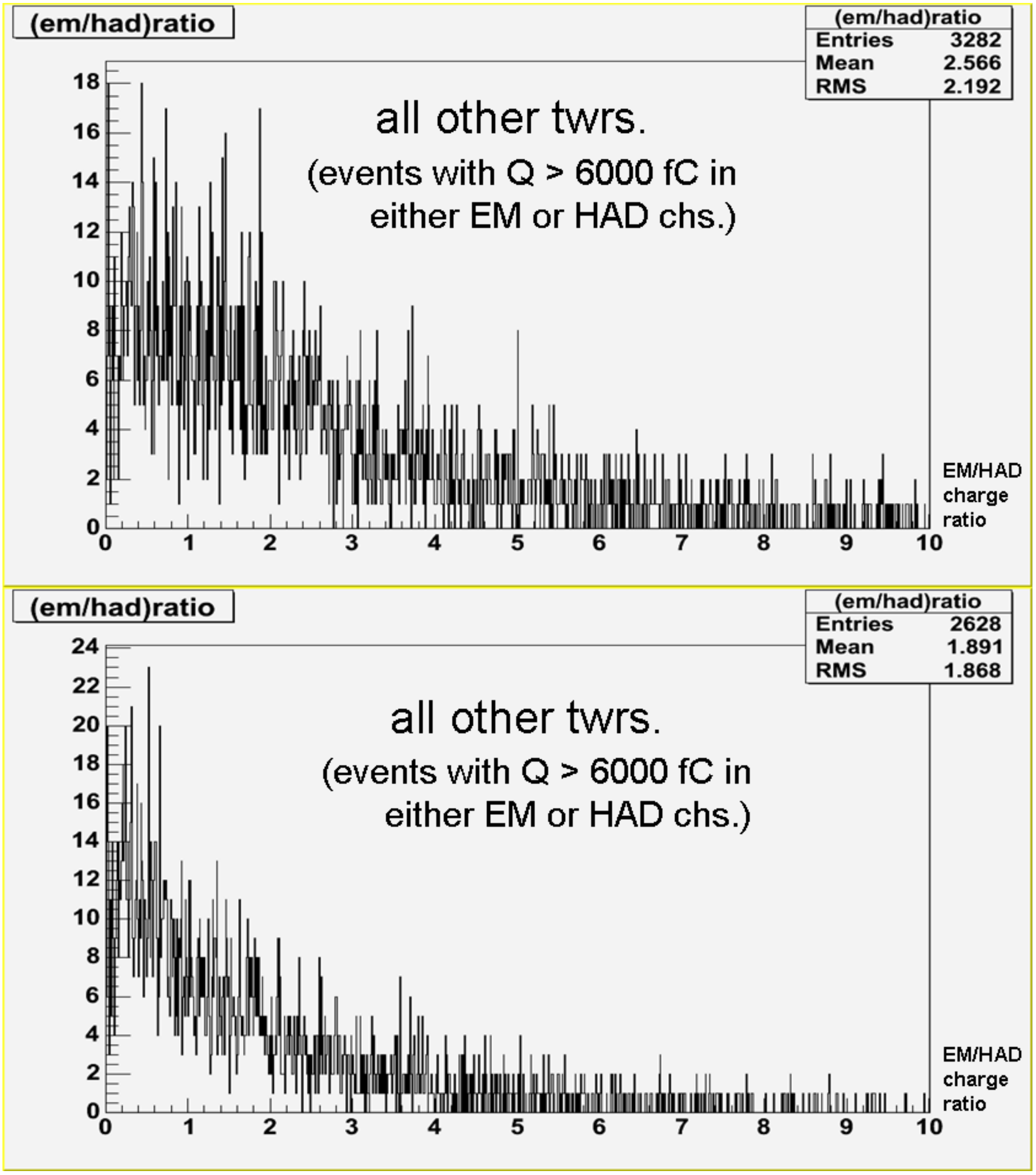

Figure 5.10. (Top) EM/HAD ratio histogram calculated with raw charge values. (Bottom) The same ratio histogram calculated with normalized EM charge values. 300 GeV pion run (run no: 15030). Plotted for the sum of all other towers.

6. CONCLUSION

The anomalous signals that are the subject of this thesis seem to have a systematical nature that is deducible but unpreventable. In other words, it is impossible to prevent shower products from directly hitting the PMTs. Yet, since the anomalous events represent non-physical experimental data, it is possible to disregard them altogether.

The main body of the analysis consists of the classification of events according to whether they are detected in the tower the test beam was incident on or in other towers, and whether they are within a reasonable energy range with respect to the energy of the test beam or above a certain value. The histograms and scatter diagrams in the analyses were plotted for many pion test runs incident on different towers. In addition to the pion plots, some additional muon plots can be found in Appendix A. The tower geometry and position of the RBXs is an important factor and it should be noted that the anomalous events were more in number in the lowermost towers of the tested wedges. (Figure 6.1.)

The final part of the analysis in which EM/HAD and HAD/EM signal ratio histograms are plotted proves especially useful in showing the relation between the channels of an event. The already established fact that real events generate comparable

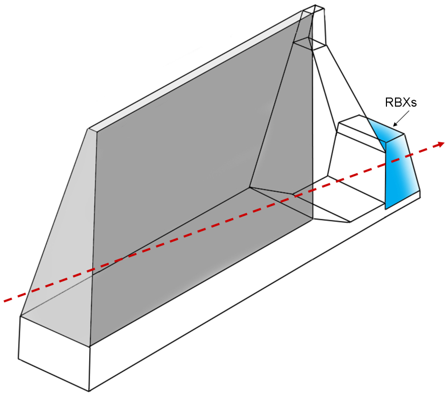

Figure 6.1. Schematic diagram of an HF wedge. Notice the position of the readout boxes and the particles passing through them.

signals in both the electromagnetic and hadronic channels is justified in the incident tower histograms. The observation that such a relation is not valid for the anomalous events may help us conclude that these events are in fact insignificant experimentally and may be discarded in the actual analyses.

APPENDIX A: ADDITIONAL HISTOGRAMS AND SCATTER DIAGRAMS

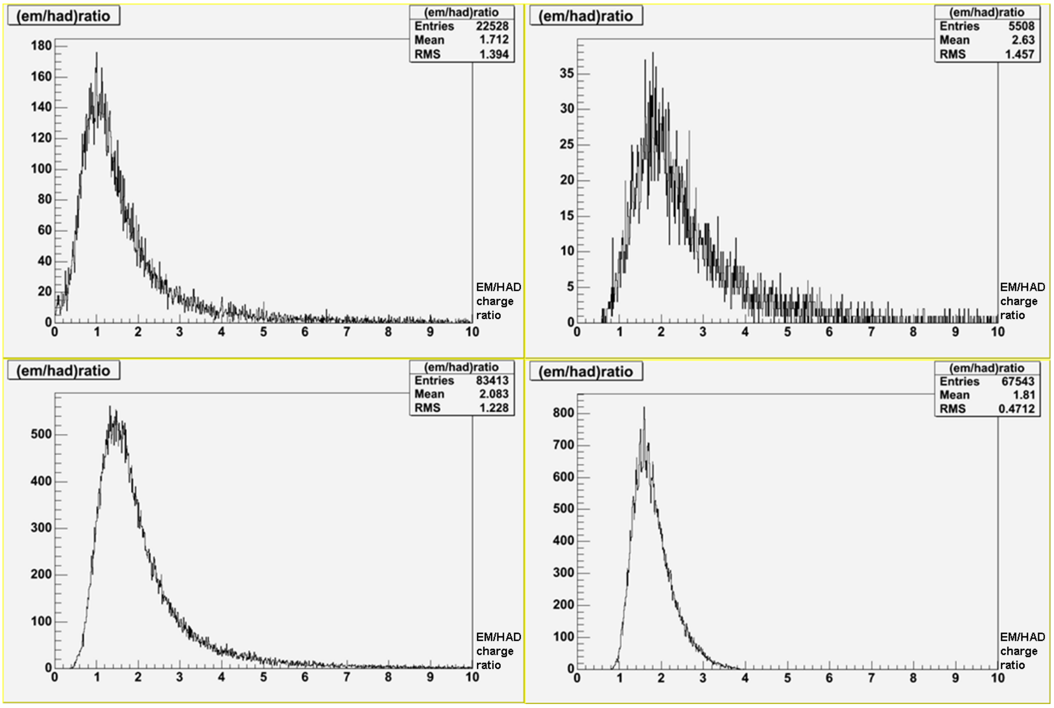

Figure A.1. EM/HAD signal ratio histograms of (clockwise from top left) 150 GeV muon beam incident on tower 2, 300 GeV pion beam incident on tower 13, 150 GeV pion beam incident on tower 4, 300 GeV pion beam incident on tower 16.

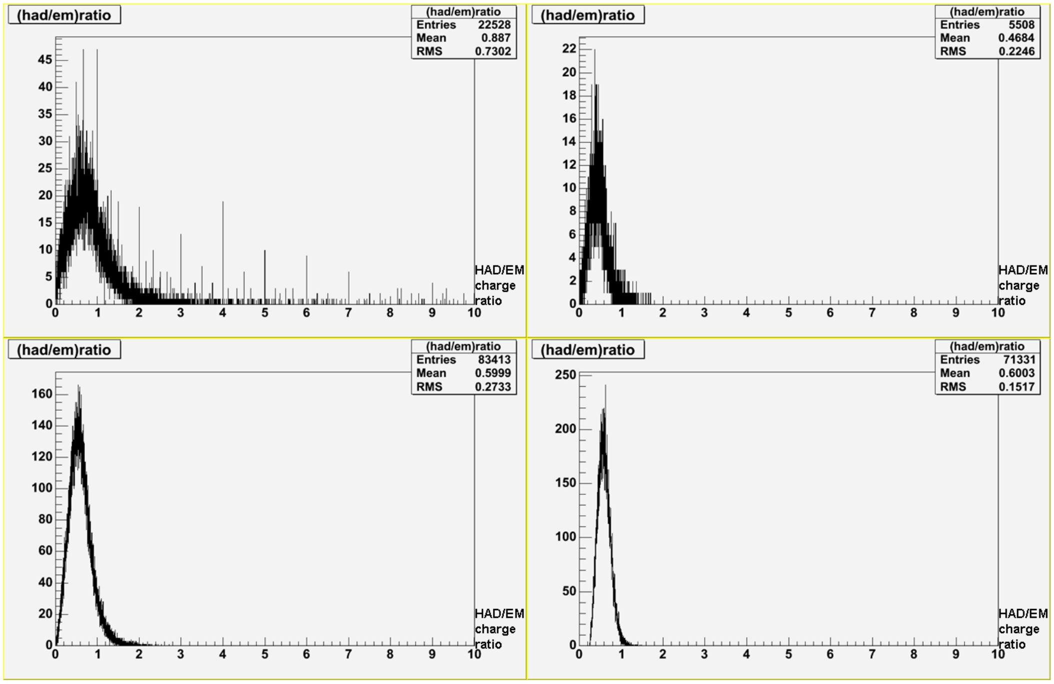

Figure A.2. HAD/EM signal ratio histograms of (clockwise from top left) 150 GeV muon beam incident on tower 2, 300 GeV pion beam incident on tower 13, 150 GeV pion beam incident on tower 4, 300 GeV pion beam incident on tower 16.

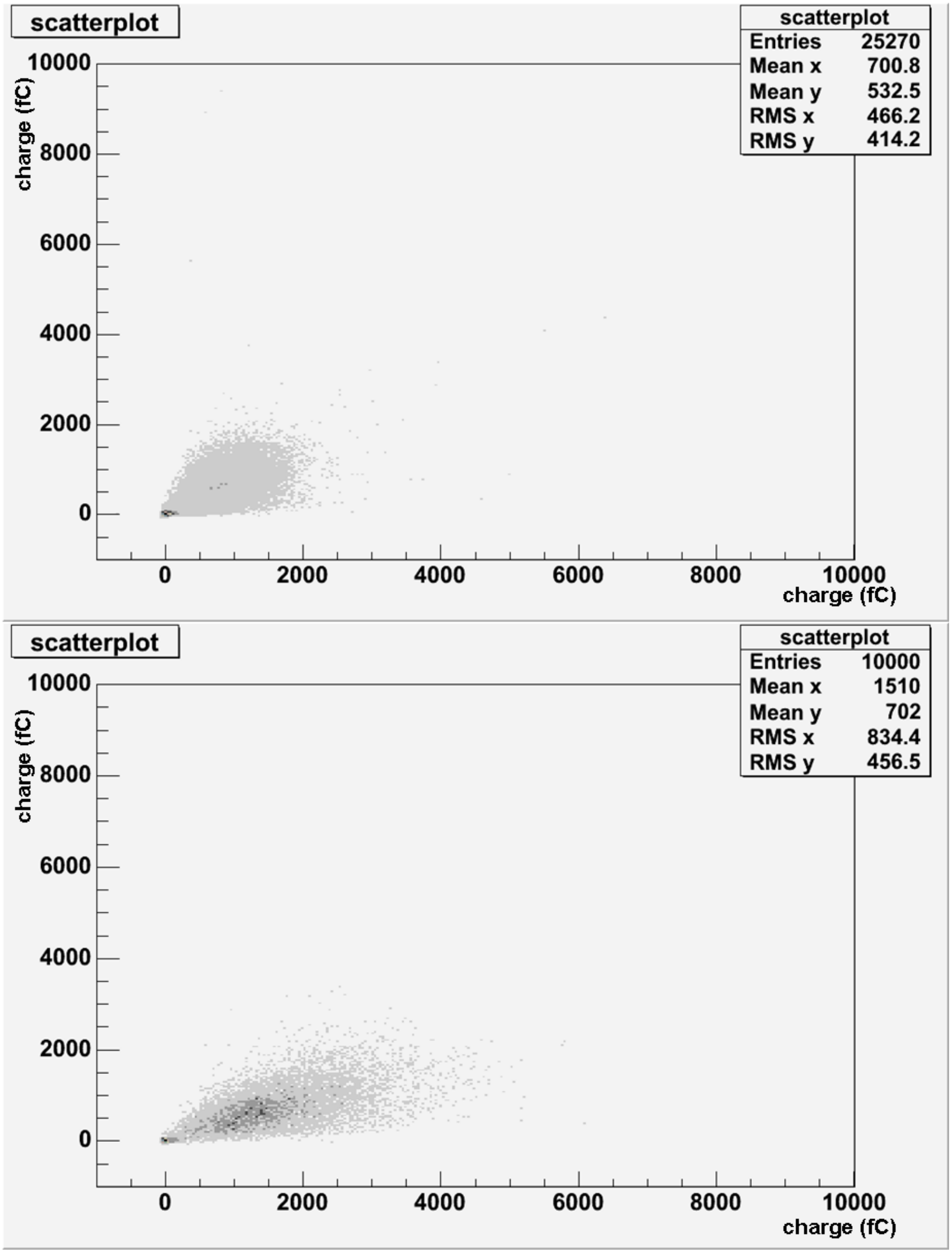

Figure A.3. Scatter diagrams for the incident tower with EM channel on the x-axis and HAD channel on the y-axis. 150 GeV muon beam incident on tower 2 and 300 GeV pion beam incident on tower 13.

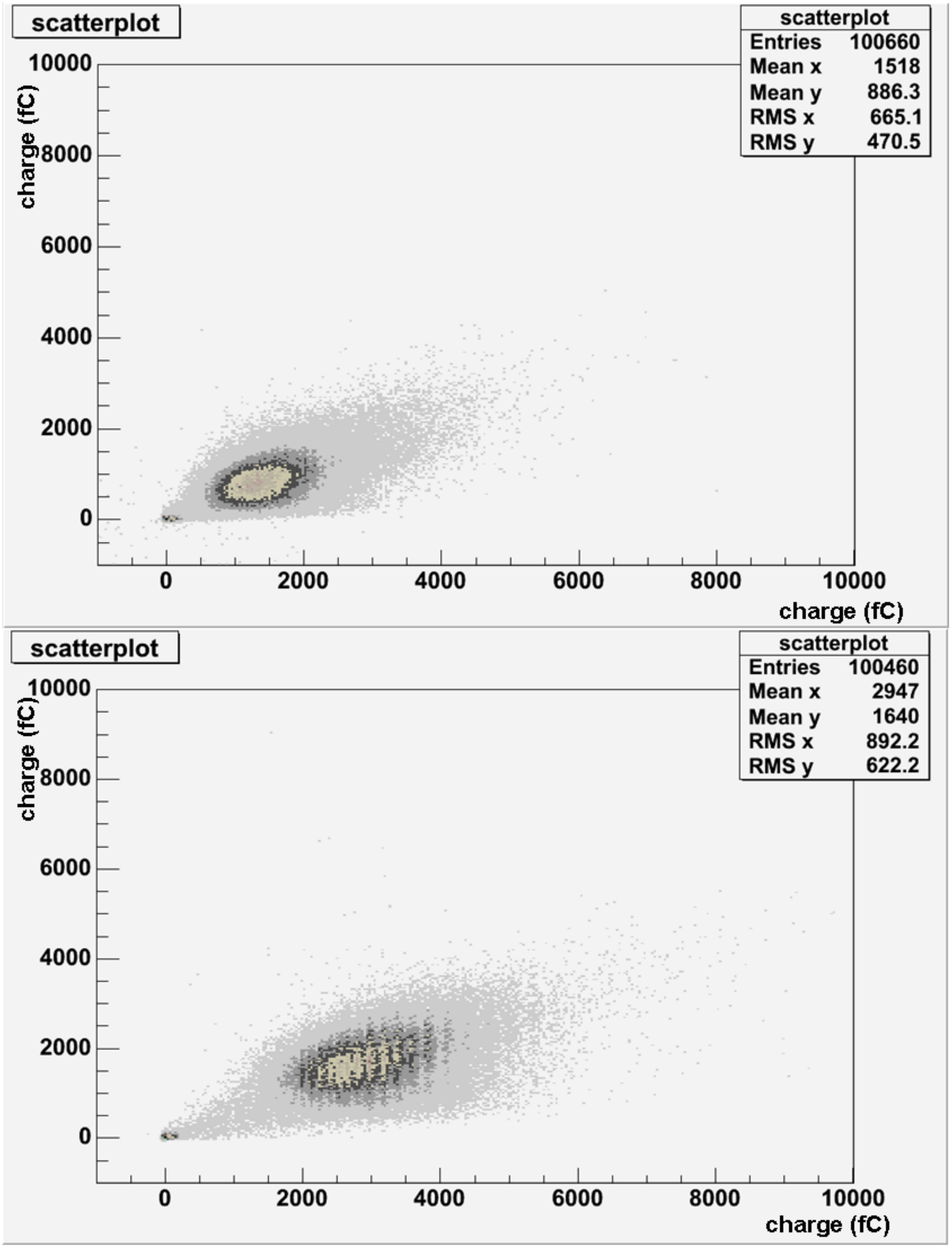

Figure A.4. Scatter diagrams for the incident tower with EM channel on the x-axis and HAD channel on the y-axis. 150 GeV pion beam incident on tower 4, 300 GeV pion beam incident on tower 16.

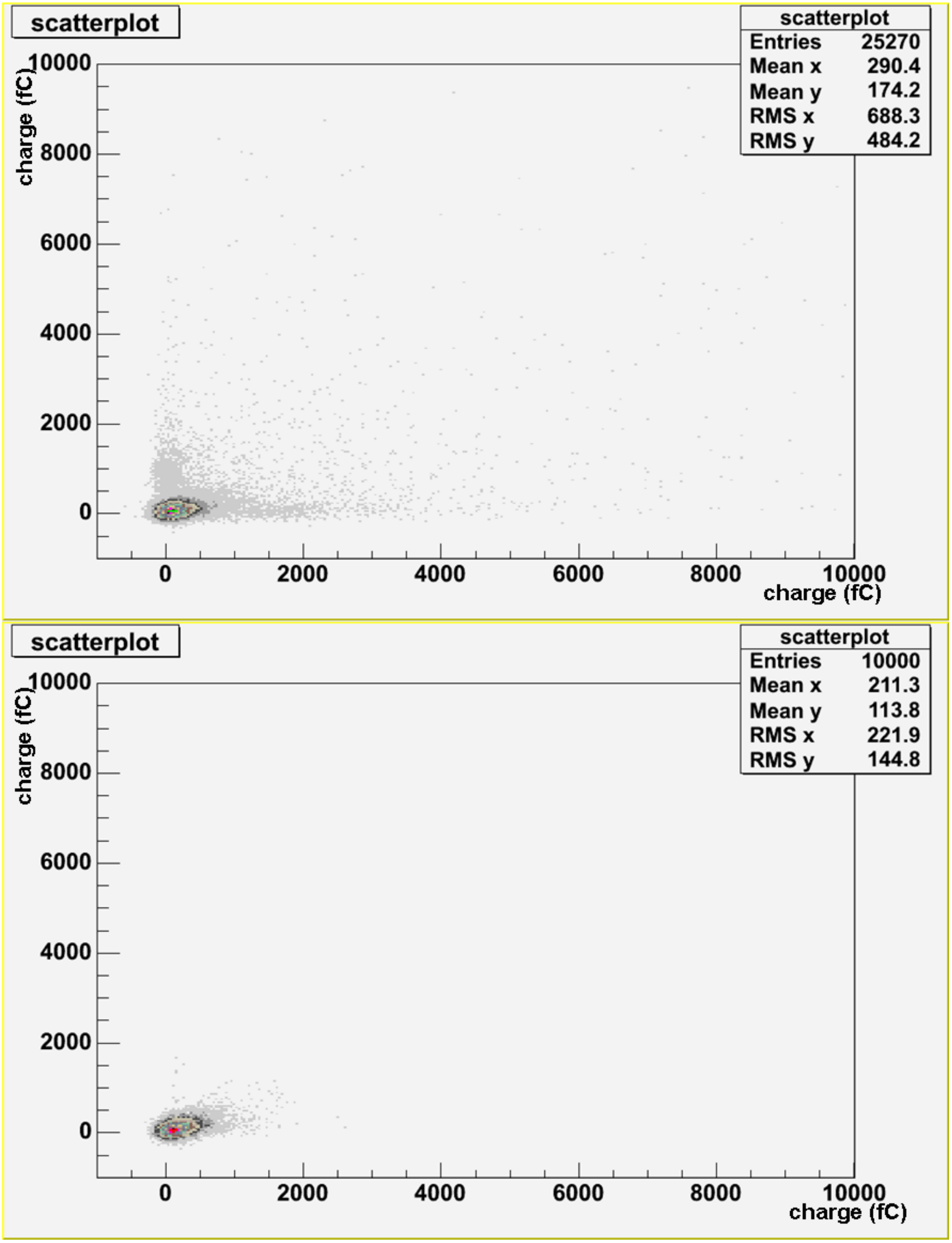

Figure A.5. All-other-towers scatter diagrams with EM channel on the x-axis and HAD channel on the y-axis. 150 GeV muon beam incident on tower 2 and 300 GeV pion beam incident on tower 13.

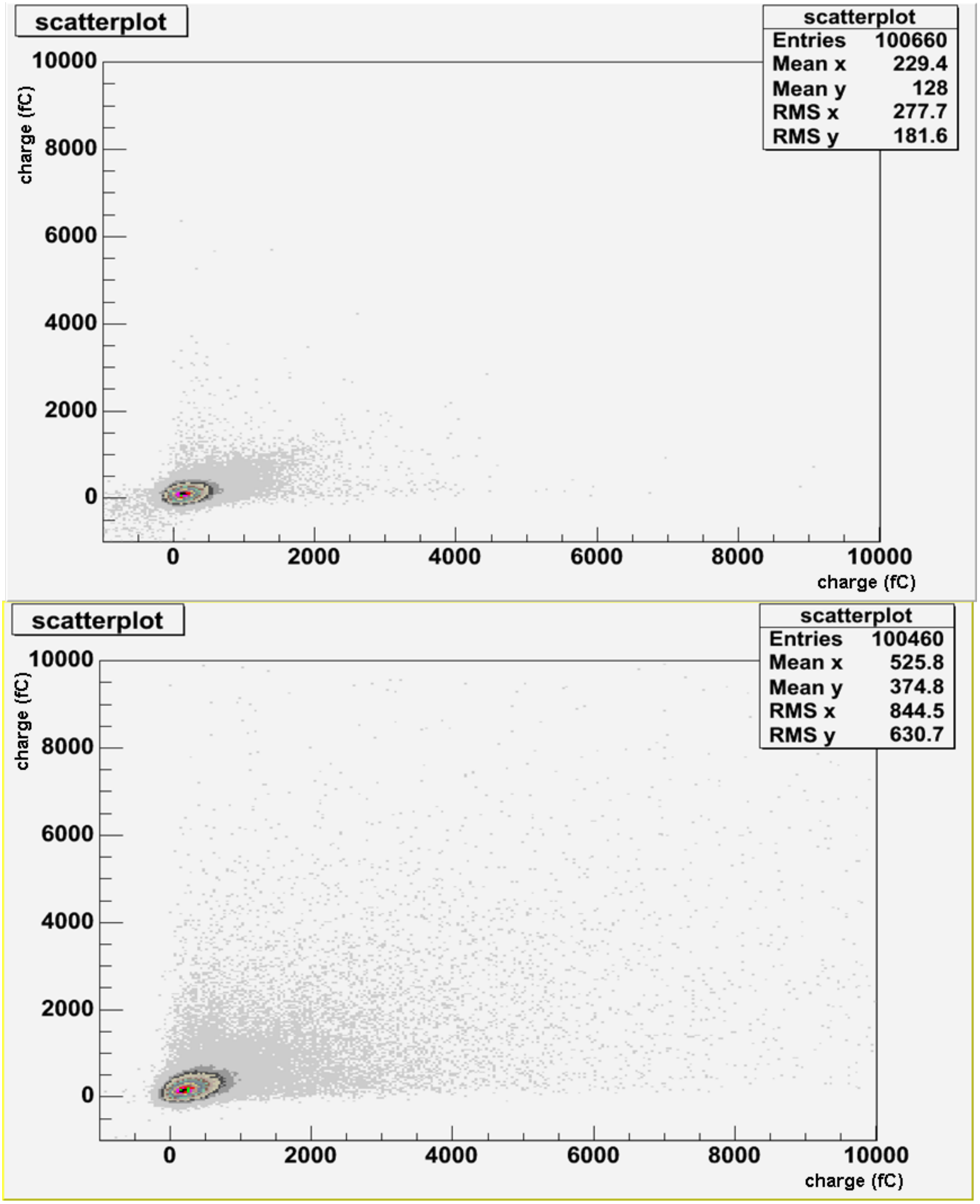

Figure A.6. All-other-towers scatter diagrams with EM channel on the x-axis and HAD channel on the y-axis. 150 GeV pion beam incident on tower 4 and 300 GeV pion beam incident on tower 16.

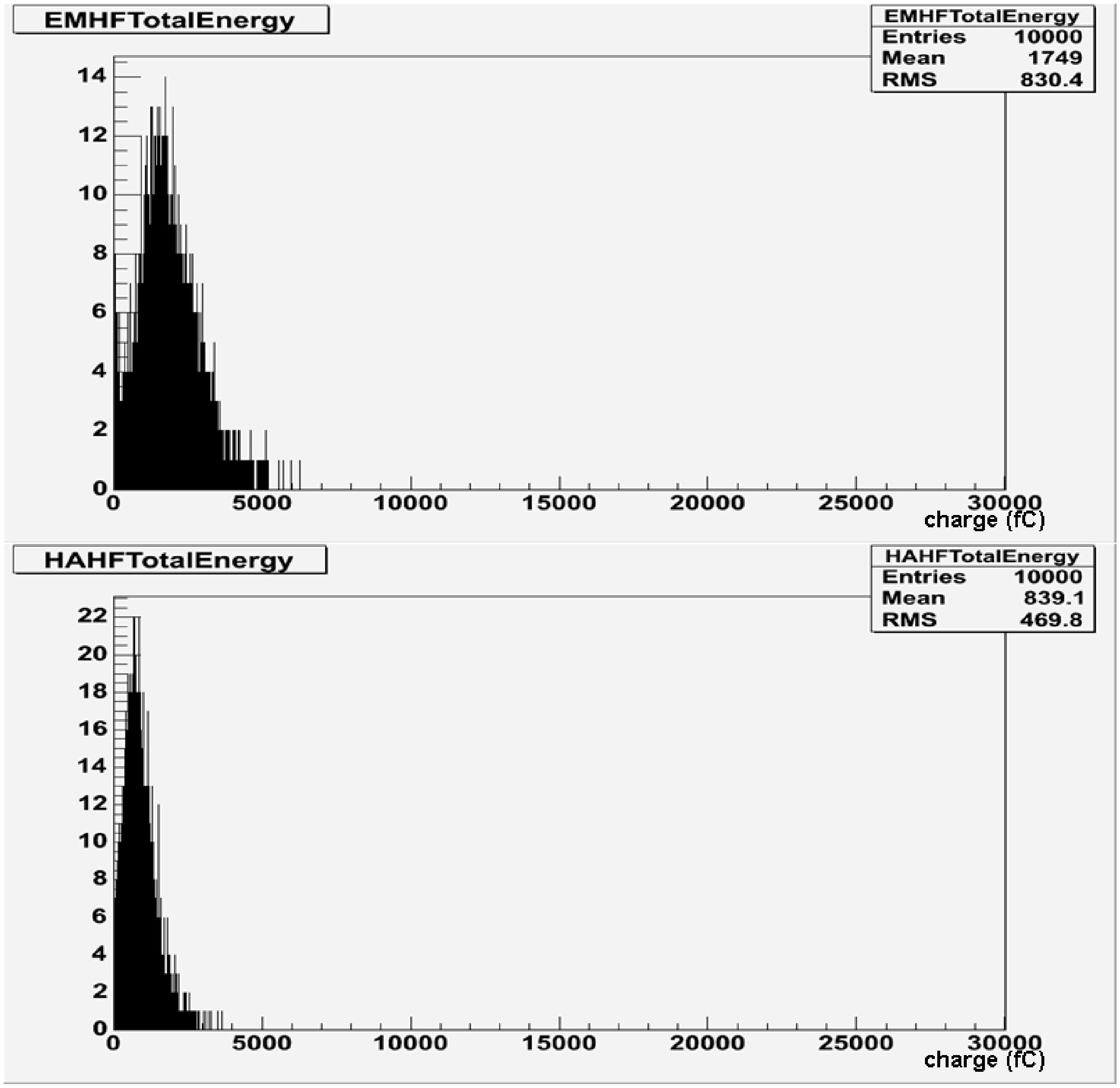

Figure A.7. Overall EM channel and HAD channel signals (meaning the sum of all towers) respectively, for a 150 GeV muon beam incident on tower 2.

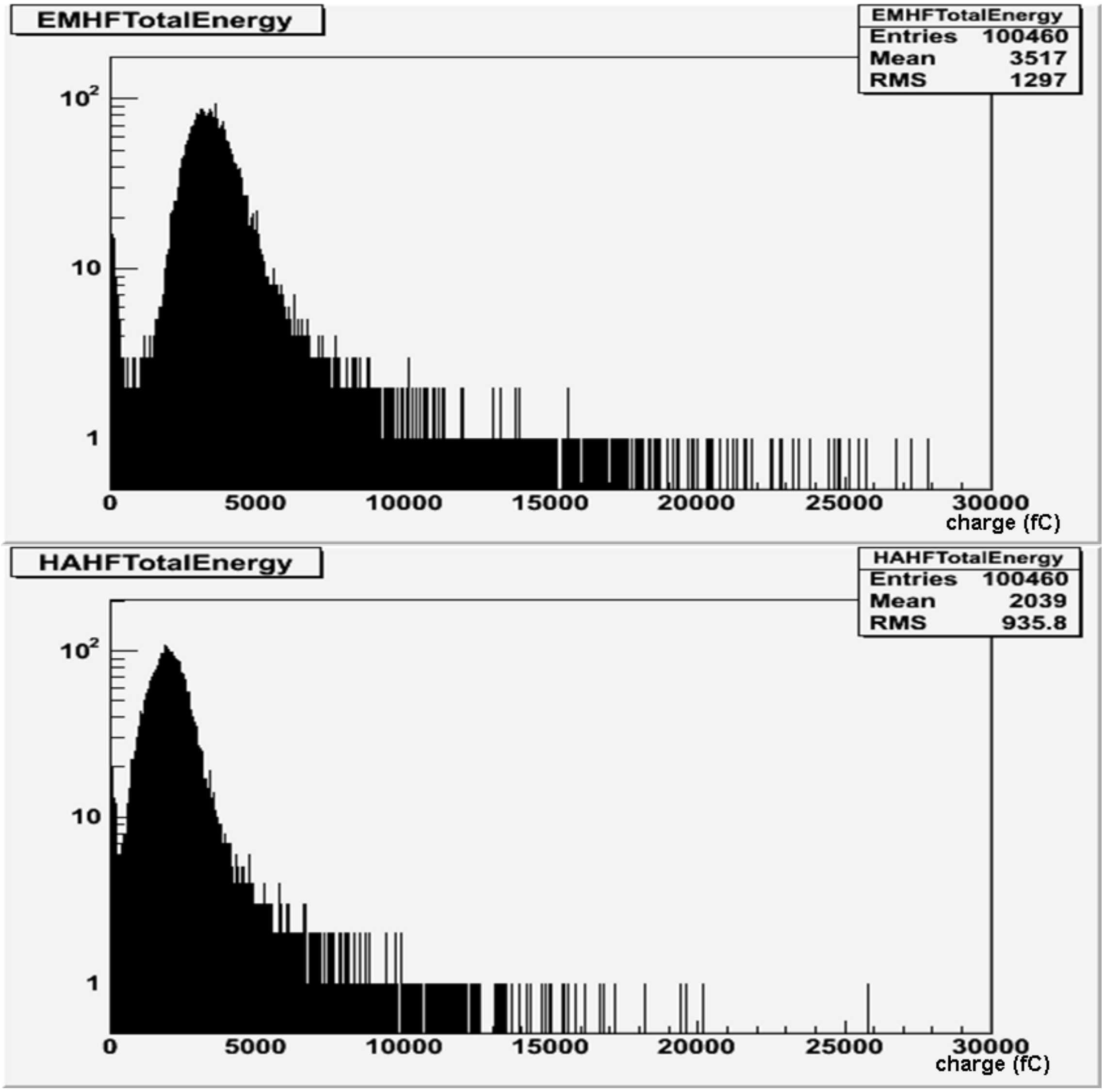

Figure A.8. Overall EM channel and HAD channel signals (meaning the sum of all towers) respectively, for a 300 GeV pion beam incident on tower 16.

APPENDIX B: EMHADRATIOINCIDENT.C

```
#include <HFTowers.hh>
#include <utils.hh>



void emhadratioincident() {
  printf("\n\n");
  printf("Usage:\n");
  printf("------\n\n");
  printf("emhadratioincident(   (int) run number,\n");
  printf("  (optional) (char) tower type,\n");
  printf("  (optional) (int) number of events )\n");
  printf("\n");
  printf("Examples:\n");
  printf("---------\n");
  printf("emhadratioincident( 13282 )\n");
  printf("emhadratioincident( 13283, \"em\", 1000 )\n");
  printf("\n");
  printf("Defaults:\n");
  printf("---------\n");
  printf("tower type       ---> em\n");
  printf("number of events ---> 1000\n");
  printf("\n");
  printf("Notes:\n");
  printf("------\n");
  printf("The available tower types are: \"em\" and \"ha\".\n");
  printf("\n");
}


void emhadratioincident(int runNumber, int cn, TString towerType="em",
```

```
 int maxEvents=1000, bool makePlot=true) {



  int EM_HA = 999;
  towerType.ToLower();
  if( !strcmp(towerType.Data(), "em") ) {
    EM_HA = _EM_;
  }
  else if( !strcmp(towerType.Data(), "ha") ) {
    EM_HA = _HA_;
  }
  else {
    cout << "Tower type not specified correctly: " << towerType.Data()
<< endl << endl;

    return;
  }

  gDirectory->DeleteAll();
  gROOT->LoadMacro("basics.cc");
  float ele[10];
  float had[10];
  float ratio[10];
  towerType.ToUpper();

  TH1F *hatestedem;
  TH1F *time[20];
  TH1F *pulses[_TOWERS_];
  TH1F *tpulses[_TOWERS_];
  TH1F *totalEnergy;
  TH2F *totPulses, *mTiming;
  TH2F *tsScatter;
```

```
for( int i = 0; i < _TOWERS_; i++ ) {
  char s[50];
  sprintf(s,"%sTower%dpedestalsubtracted",towerType.Data(),i+1);
  pulses[i] = new TH1F( s, s, 20, -0.5, 19.5 );
  pulses[i]->GetXaxis()->SetTitle("time slice");
  if( i < 20 ) {
    sprintf( s, "%d.timeslice", i+1 );
    time[i] = new TH1F( s,s, 10000, 0, 10000);
  }
  sprintf(s,"%sTower%dtotalchargepedestalsubtracted",
  towerType.Data(),i+1);

  tpulses[i] = new TH1F( s, s, 1000, 0, 4000 );
  tpulses[i]->GetXaxis()->SetTitle("charge (fC)");
  }

char d[30];
sprintf( d, "scatterplot");
tsScatter = new TH2F( d, d, 300, -1000, 10000, 300, -1000, 10000 );

sprintf( d, "(em/had)ratio" );
hatestedem = new TH1F(d, d, 1000, 0, 10);

sprintf(s,"%sHFTotalPulsesMap",towerType.Data());
totPulses = new TH2F( s, s, 2, 0, 2, 13, 1, 14 );
sprintf(s,"%sHFMeanTimingMap",towerType.Data());
mTiming = new TH2F( s, s, 2, 0, 2, 13, 1, 14 );
sprintf(s,"%sHFTotalEnergy", towerType.Data());
totalEnergy = new TH1F( s, s, 1000, 0, 4000 );
```

```
DCCData* dcc;
HFTowers *hf = new HFTowers();

unsigned short buffer[25];
double data[20];
char fiber, qieid, er, dv, cap, qie;

char filename[200];
//  sprintf(filename,"/tmp/HTB_%06d.root",runNumber);
sprintf(filename,"/data/HTB_%06d.root",runNumber);
if( gSystem->AccessPathName(filename) ) {
  cout << endl << "File: " << filename << " not there!!!" << endl
   << endl;

  return;
}
else ;
TestBeamDataFile f;
f.load(filename);

double totEvents = f.getNEvents();
cout<<"there are "<<totEvents<<" events in this run"<<endl;
int nEvents = 0;
int goodEvents = 0;
int badCaps = 0;
int hardInfo[2] = {999,999};

while( f.getNextEvent() && nEvents++ < maxEvents ) {
  dcc = f.getEventData()->getHCALData()->getDCC(_DCC_);
  float tenergy=0.;

  ele[1]=0;
```

```
    had[1]=0;

    for(int ntower = cn; ntower <= cn; ntower++) {
      float eenergy=0.;


      for(int a=0; a<2; a++){

if(a==0) {EM_HA=_EM_; hf->decode2hardware( EM_HA, ntower, hardInfo );}
if(a==1) {EM_HA=_HA_; hf->decode2hardware( EM_HA, ntower, hardInfo );}

dcc->getQIEData( hardInfo[0], hardInfo[1], buffer );
      // check caps (function in basics.cc) //
      bool capok = isCapOK( buffer );
      float pedestal = estimatePedestal_noninv( dcc, buffer );
      // float pedestal = 0;//
      bool hasAP = false;
      if( capok ) {


for(int tslice = 0; tslice < 20; tslice++) {
  DCCData::parseQIE(buffer[tslice],fiber,qieid, er, dv, cap, qie);
  //data[tslice] = dcc->convert2fC(qie)-pedestal;
  data[tslice] = dcc->convertToFC_noninv(qie)-pedestal;

  if (ntower == cn){


    if (a == 0) ele[1]+=data[tslice];
    if (a == 1) had[1]+=data[tslice];
```

```
  pulses[ntower-1]->Fill( tslice, data[tslice] );
  eenergy += data[tslice];
  goodEvents++;
  }

tpulses[ntower-1]->Fill( eenergy );
tenergy += eenergy;
}
      }
      else {
badCaps++;
      }
      }

       totalEnergy->Fill( tenergy );

    }
     tsScatter ->Fill( ele[1], had[1] );

     if (had[1] != 0) ratio[1] = ele[1]/had[1];

     if ( had[1] > 750 && 3000 > had[1] ){
       if ( ele[1] > 1500 && 4000 > ele[1] )
 hatestedem -> Fill( ratio[1] );}
  }

  goodEvents /= (20*24); // <--- divide by number of channels and time
  slices

  cout << "Processed " << nEvents << " events and " << goodEvents <<
  " good events." << endl;
```

```
cout << "There were " << badCaps << " bad caps." << endl;
f.close();

float gtheTowers[_TOWERS_];
float gttiming[_TOWERS_], gttimRMS[_TOWERS_];
float gmeans[_TOWERS_], gmeansRMS[_TOWERS_];

for( int aps = 0; aps < _TOWERS_; aps++ ) {
  if( pulses[aps]->GetEntries() )
    pulses[aps]->Scale( 20./pulses[aps]->GetEntries() );
  else ;

  if( aps+1 < 12 ) {
    totPulses->Fill( 0, aps+1, pulses[aps]->Integral() );
    mTiming  ->Fill( 0, aps+1, pulses[aps]->GetMean() );
  }
  else if( aps+1 > 13 ) {
    totPulses->Fill( 1, (aps+1)-13, pulses[aps]->Integral() );
    mTiming  ->Fill( 1, (aps+1)-13, pulses[aps]->GetMean() );
  }
  else if( aps+1 == 12 || aps+1 == 13 ) {
    totPulses->Fill( 0, aps+1, pulses[aps]->Integral() );
    totPulses->Fill( 1, aps+1, pulses[aps]->Integral() );
    mTiming  ->Fill( 0, aps+1, pulses[aps]->GetMean() );
    mTiming  ->Fill( 1, aps+1, pulses[aps]->GetMean() );
  }
  else ;
  gtheTowers[aps] = aps+1;
  gttiming[aps]   = pulses[aps]->GetMean();
  gttimRMS[aps]   = pulses[aps]->GetRMS();
  gmeans[aps]     = tpulses[aps]->GetMean();
  gmeansRMS[aps]  = tpulses[aps]->GetRMS();
```

```
    }
  /// ***************************************************************

  TGraph *gr_means = new TGraph( _TOWERS_, gtheTowers, gmeans );
  gr_means->SetTitle("mean of pulses");
  gr_means->SetMarkerStyle(20); gr_means->SetMarkerSize(1);
  TGraph *gr_meRMS = new TGraph( _TOWERS_, gtheTowers, gmeansRMS );
  gr_meRMS->SetTitle("RMS of pulses");
  gr_meRMS->SetMarkerStyle(20); gr_meRMS->SetMarkerSize(1);
  TGraph *gr_timing = new TGraph( _TOWERS_, gtheTowers, gttiming );
  gr_timing->SetTitle("mean of timing");
  gr_timing->SetMarkerStyle(20); gr_timing->SetMarkerSize(1);
  TGraph *gr_timRMS = new TGraph( _TOWERS_, gtheTowers, gttimRMS );
  gr_timRMS->SetTitle("RMS of timing");
  gr_timRMS->SetMarkerStyle(20); gr_timRMS->SetMarkerSize(1);

  if( makePlot ) {
    TCanvas* c20= new TCanvas("time slice scatter","time slice
    scatterer");

    //c20->Divide(1,1);
    tsScatter->SetOption("col");
    tsScatter->Draw();

    TCanvas* cHaTestedEm = new TCanvas("cHaTestedEm", "energy");
    hatestedem->Draw();
  }
}
```

REFERENCES

1. Moeller A. et al., *Analysis of abnormally high energy events in CMS forward calorimeters*, CMS Internal Notes, CMS IN-2008/014, 2008.

2. Hunt A. et al., *Test beam 2007 results of the anomalous signals in CMS-HF PMTs*, CMS Contributions/Talks, April 2008.

3. *LHC: The Guide*, CERN, CERN-Brochure-2008-001-Eng, 2008.

4. *CMS Physics: Technical Design Report Vol. 1 Detector Performance and Software*, CMS Collaboration, 2006.

5. Chatrchyan S. et al. and CMS Collaboration, "The CMS Experiment at the LHC", *Journal of Instrumentation*, Vol. 3, Number 08, 2008.

6. http://cms-project-cmsinfo.web.cern.ch/cms-project-cmsinfo, 2008.

7. Weatherall J. O., *The Accidental Particle*, http://www.slate.com/id/2199573/pagenum/all, 2008.

8. *Introduction to Supersymmetry*, http://hitoshi.berkeley.edu/public_html/susy/susy.html, 2008.

9. http://theory.caltech.edu/people/jhs/strings/str121.html, 2008.

10. http://www.darkmatterphysics.com, 2007.

11. http://www.superstringtheory.com, 2008.

12. Wigmans R., *Calorimetry*, Oxford University Press, New York, 2000.

13. Green D., *The Physics of Particle Detectors*, Cambridge University Press, Cam-

bridge, 2000.

14. “Design, performance, and calibration of CMS forward calorimeter wedges” , CMS-HCAL Collaboration, *Eur. Phys. J.* C 53, 2008, 139-166.

15. Brun R. et al., *Root User’s Guide 5.16*, CERN, 2007.

16. Halu A., E. Gülmez and M. Deliömeroğlu, *A study of anomalous events in CMS-HF PMTs*, CMS Conference Report, CMS CR-2008/107, 2008. (To be published in *Proceedings of the International Conference on Particle Physics*, İstanbul, October 27-31, 2008, Balkan Physics Letters.)